AD

RSIC-535

TRANSPIRATION AND FILM COOLING OF LIQUID ROCKET NOZZLES

GPO PRICE $ _____

CFSTI PRICE(S) $ _____

Hard copy (HC) 3.00

Microfiche (MF) .75

ff 653 July 65

by
John E. Terry
Gus J. Caras

March 1966

DISTRIBUTION OF THIS DOCUMENT IS UNLIMITED

REDSTONE SCIENTIFIC INFORMATION CENTER
REDSTONE ARSENAL, ALABAMA

JOINTLY SUPPORTED BY

U.S. ARMY MISSILE COMMAND

GEORGE C. MARSHALL SPACE FLIGHT CENTER

31 March 1966 RSIC-535

TRANSPIRATION AND FILM COOLING OF LIQUID ROCKET NOZZLES

by
John E. Terry
Gus J. Caras

DISTRIBUTION OF THIS DOCUMENT IS UNLIMITED

Research Branch
Redstone Scientific Information Center
Research and Development Directorate
U. S. Army Missile Command
Redstone Arsenal, Alabama 35809

ABSTRACT

This report presents a summary of current theoretical and experimental work conducted on transpiration and film cooling of rocket nozzles. An effort was made to assess the present technology to bring the reader abreast of the general status of these cooling techniques. Major problems which exist in developing transpiration and film cooling are presented in the conclusions.

The discussion of various aspects of transpiration and film cooling is not meant to be exhaustive. Its purpose is to provide a background for the reader who is interested in further pursuing these cooling techniques.

FOREWORD

This report presents a summary of the pertinent literature published primarily since 1960 on transpiration and film cooling. Theory and analytical procedures which have been developed and experimental effort which has been devoted to the rocket nozzle cooling techniques are reviewed and, where possible, compared. Those theoretical approaches which are best substantiated by experiment and useful for propulsion application are pointed out where sufficient information is available to make this decision. An effort has been made to determine the status of the technology, pointing out critical gaps, if any, which still exist.

The following sources of information available at the Redstone Scientific Information Center were searched primarily for the period from 1960 to the present.

1) Redstone Scientific Information Center holdings (books, reports, and journals).
2) NASA (a computer tape search of NASA tapes which contain references from the Scientific and Technical Aerospace Reports and the International Aerospace Abstracts).
3) Defense Documentation Center (pertinent references and documents furnished by Defense Documentation Center).

CONTENTS

ILLUSTRATIONS

Section I. INTRODUCTION

Recent advances in rocket motor development have intensified the problem of effectively cooling the nozzle operating under conditions of high, local heat flux. Motor development advances have proceeded at a faster rate than material technology to the point where uncooled materials cannot withstand the environment now capable of being generated. For this reason, cooled nozzle designs become necessary, even though cooling systems usually add weight to the rocket and sometimes penalize the performance.

Regenerative (convection) cooling has been used successfully on SATURN, TITAN, ATLAS, etc., but this method provides for a maximum heat dissipation on the order of 5000 Btu/ft^2-sec, which can be easily exceeded in a rocket nozzle.[1] Dump cooling is limited because its maximum heat dissipation is about 1500 Btu/ft^2-sec.[2] Ablation cooling is quite attractive, particularly for engines which can be throttled, but controlling the fabrication process and obtaining reproducible properties for the char and virgin material have proved to be difficult.[2] Further, the maximum heat dissipation currently provided by ablation cooling is about 500 Btu/ft^2-sec. Heat sink cooling is simple and inexpensive, but this cooling method is limited to a firing duration of only a few seconds at high heat flux conditions.

From the many studies that have been made on rocket nozzle cooling, it is generally agreed that film and transpiration type cooling will be necessary for the increasingly more severe nozzle environments being considered. These studies have indicated that on the basis of equal coolant flow rates, transpiration cooling provides the most effective performance under severe operating conditions. This is shown in Figure 1. Despite the fact that extensive investigations have been devoted to film and transpiration cooling, practical application of these methods to high performance rocket engines is meeting with some development difficulties. In transpiration cooling, the major problem in application is to achieve very small, closely spaced passages through which the coolant will flow.[3] In liquid film cooling, additional work is required in film stability and in determining the most feasible velocity ratio of injected coolant to free stream gas.[4]

Design requirements for future combustion chambers will likely dictate the use of a combination of two or more cooling methods. Some cooling combinations which are promising are film/heat sink, transpiration/heat sink, film/radiation, transpiration/radiation, film/ablation, transpiration/ablation, film/regenerative, transpiration/regenerative,

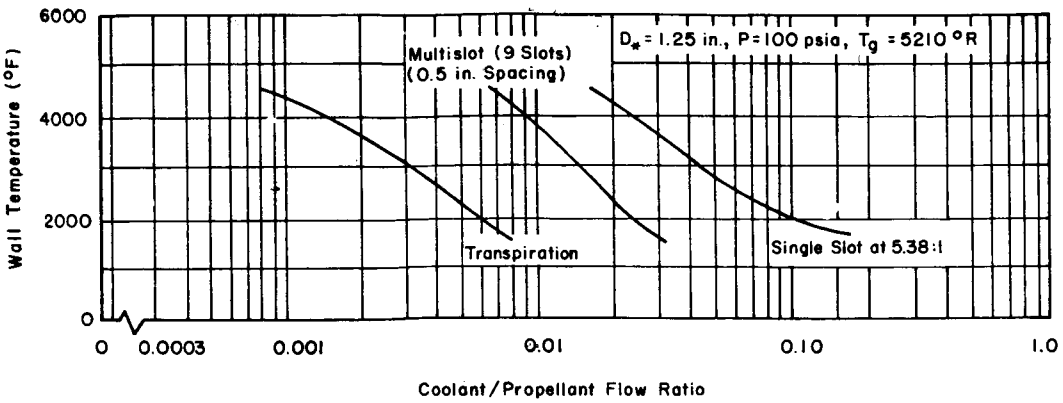

Figure 1. Comparison of Cooling Techniques for Nozzles - O_2/H_2 Fuel and H_2 Coolant[5]

transpiration/film, and radiation/heat sink.[3, 5] Combinations of regenerative-film cooling and ablative-film cooling have been used successfully on several engines,[6] but no production engines utilizing only film or transpiration cooling for the nozzle operating at high temperatures are known to exist.

This report is concerned with a summary of the current theoretical and experimental studies on transpiration and film cooling. No attempt has been made to discuss in detail all the extensive work that has been devoted to these cooling techniques but only the highlights of some of the most notable work that is currently being used in development. Also, an effort has been made to define the major problems which still exist in developing these cooling techniques. Transpiration or film cooling combined with other cooling techniques has not been evaluated because most of these combinations deserve separate, extensive surveys. As may be expected, combining cooling methods compounds the complexity of analytical analyses.

Since self-cooling is in essence a type of transpiration cooling, a discussion on this cooling method is included in Section II on transpiration cooling. The literature indicates that development in self-cooling has been for solid rockets using high-energy metallized propellants, and no indication was found that it is to be applied to liquid rocket cooling. However, there is no known reason why self-cooling cannot be applied to cooling of liquid as well as solid rocket nozzles.

Section II. TRANSPIRATION COOLING

1. Status of Transpiration Cooling

Transpiration is commonly defined as that process whereby a fluid transpires through a porous medium. When transpiration is used as a means of cooling, there are at least two principal heat reducing mechanisms at work. First, heat is absorbed by the cooling fluid as it travels against the direction of heat flow from some reservoir to a surface of higher temperature and consequently lowers the wall temperature; and, second, as the fluid emerges from the surface of the wall, it forms an insulating layer between the surface of the wall and the hot gas.

Figure 2 shows one of the methods of achieving transpiration cooling. In this method, the wall is manufactured from a porous material and the coolant is blown through the pores. The coolant film on the hot-gas side is, therefore, continuously renewed and the cooling effectiveness can be made to stay constant along the surface. When a liquid is used as a coolant, a liquid film is created on the hot-gas side which is evaporated on its surface, and the heat absorbed by the evaporation process increases the cooling effectiveness. This process is frequently referred to in the literature as evaporative-transpiration cooling.[7]

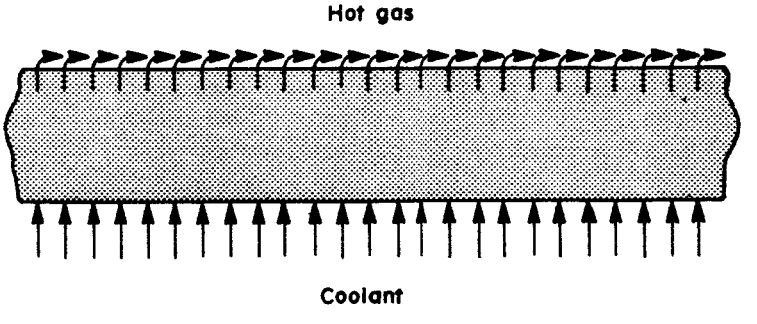

Figure 2. Transpiration Cooling

Another type of transpiration cooling consists of a porous refractory matrix which is filled with a material that vaporizes in service to provide protective heat sink and/or gaseous thermal barrier (Figure 3). Although this type of cooling has been investigated specifically for solid rocket nozzle applications, it could be used for any nozzle application where high-heat flux and long-firing duration preclude the use of an uncooled or a regeneratively cooled nozzle.[4] The matrix is usually made out of a high temperature melting material such as tungsten in which a low melting material (such as copper, silver, zinc, etc.) is infiltrated.

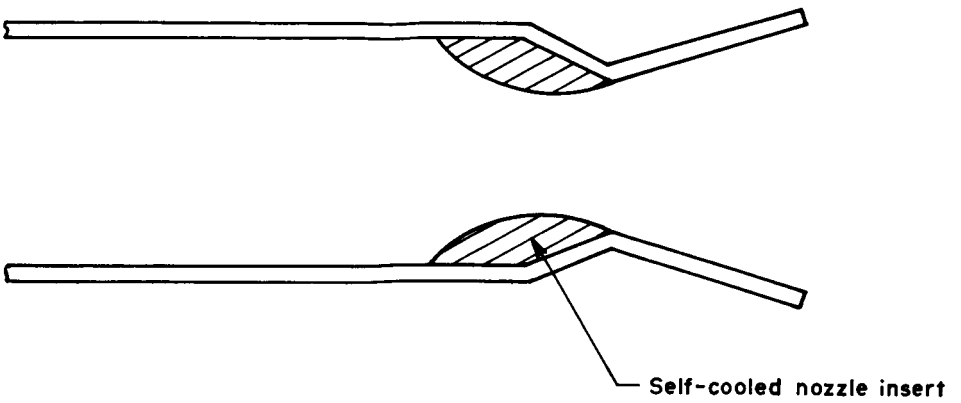

Figure 3. Self-Cooling of Rocket Nozzle

This type of cooling is frequently referred to in the literature as self-cooling or autotranspiration to distinguish from the type where the entire chamber or nozzle wall is made out of a porous material through which the coolant transpires.

Although in theory transpiration cooling provides the greatest cooling effectiveness as compared to other cooling methods, it has not been applied for cooling rocket engine nozzles. Most of the published literature deals with theoretical rather than experimental investigations. Some of the difficulties associated with the application of this cooling method are the fabrication of porous shapes with uniform porosity and the inherent weakness of large porous surfaces as compared to solid sections. To take advantage of the transpiration cooling, and also to alleviate structural problems, it is desirable to make use of a partially porous surface, since it is not necessary for all areas of an engine to be cooled. Thus, the forward surfaces, with the largest heat transfer rates, can be transpiration cooled while the rearward areas, where heating is not so severe, can be protected by the coolant film introduced into the boundary layer.[8]

Recent technological innovations include the development of sintered metals and ceramics of controlled porosity and the development of multi-layer, fine wire-mesh screens. These new techniques offer the most promising approach to achieving transpiration cooling in rocket nozzle systems.

In general, the state of development of transpiration cooling is not as advanced as that of film cooling. There are no liquid rocket nozzles today that are cooled by transpiration cooling alone or in combination with some other cooling technique. A review of the literature suggests that considerable experimental work is required not only in the area of

fabrication of porous materials and the selection of proper coolants but also in understanding the mechanisms of transpiration cooling and verifying theory. Most of the experimental work, for example, has been centered around flat surfaces and one-phase cooling which are easier to treat analytically.

2. Theoretical and Experimental Investigations

a. Wall Materials

Fabrication of porous shapes by sintering is a modern application of clay pottery technology. Practically any metal which can be reduced to a fine powder can be used. Fabrication of the porous shape is accomplished by either one of two basic processes. In the first method, suggested by Meyer-Hartwig,[7] the metal powder is mixed with a binder, formed in a mold to the desired shape and sintered in a furnace after the mold is removed. In the second technique, developed by Duwez and Martin,[9] the powdered metal is mixed with a gas-evolving compound such as ammonium bicarbonate. The mixture is then pressed into the desired shape and the pressure maintained on the material while it is sintered in a reducing (hydrogen) atmosphere. A comparison of these two methods shows the Meyer-Hartwig process permits the fabrication of an almost unlimited variation in article shape although shrinkage during sintering may cause cracking (Figure 4) or make porosity control rather difficult.[10]

The second fundamental method of fabricating a porous metal material is to use wire-mesh screens. This method can be used with any metal sufficiently ductile to be drawn into wire. The wire is woven into a cloth or gauze to the desired contour and then sintered. The porosity of the material is determined by the wire spacing.

A more recent method is based on a combination of felting techniques and powder metallurgy and appears to combine the advantages of both the powdered-metal and wire-winding techniques. In this method, metal fibers mixed with a viscous fluid are beaten into a slurry, which is then charged to a porous felting mold. Vacuum drying removes the liquid, leaving the fibers deposited on the inner mold surface, and the resulting felt is sintered. Porous metal products can be fabricated in the form of continuous sheets or in intricate shapes.

A novel concept for fabrication of wall materials for transpiration cooling was advanced by Aerojet-General Corporation.[11] This method consists of stacking together very thin washers which have been previously

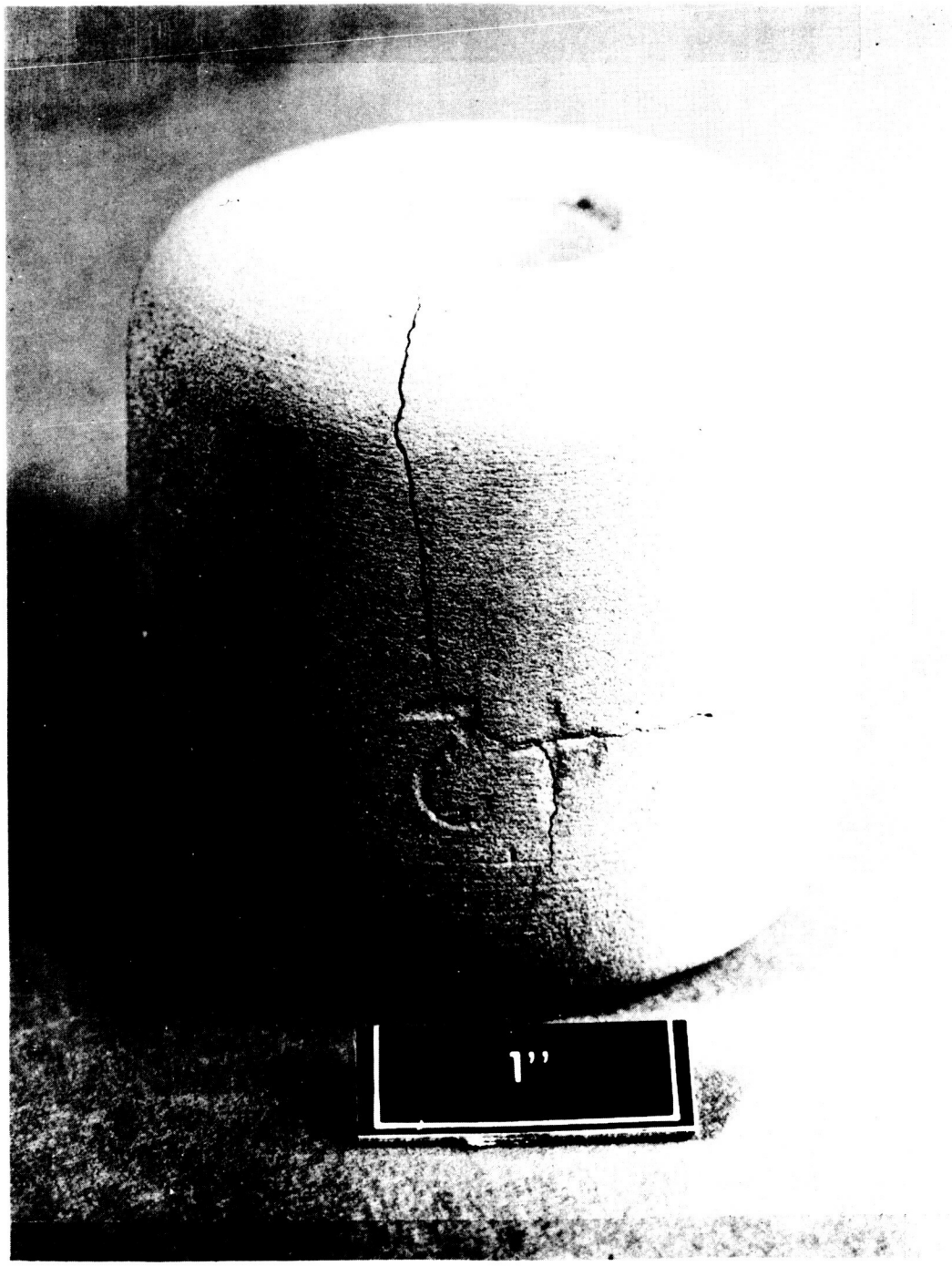

Figure 4. Cracked Outer Layer Caused by Differential Sintering Shrinkage[12]

grooved to extremely high tolerances by photoetching or chemical milling processes. After feasibility demonstration, Aerojet-General Corporation plans to design a flight-weight chamber using this concept.

Of the methods used for fabricating porous media, the wire-winding and felting techniques have the best strength qualities. Magnusson, Misra, and Thompson[10] give a more detailed review of these methods. Table I summarizes the most important advantages and disadvantages for the several types of wall materials.

In general, a material for fabrication of the porous wall must meet the following requirements:

1) It must have the necessary properties at the operating temperature to maintain its structural and dimensional integrity.
2) It must be corrosion and erosion resistant to the propellant and the coolant at operating temperatures.
3) It must be resistant to thermal shock.

Since the first criterion of any potential material in a high temperature environment is a high melting point (m. p.), the materials considered are tungsten, tantalum, molybdenum, and columbium. Most of the other refractory materials were not considered because of scarcity or because they did not offer significant advantages over the materials named above. The use of non-metallic materials presents problems in design, fabrication, and frequently incompatibility with the coolant at high temperatures.

Table II presents the pertinent properties of the refractory metals for service above 3000°F. All of these metals possess adequate corrosion and erosion resistance, are resistant to thermal shock, and have sufficient strength and ductility at elevated temperatures.

The strength-to-weight ratios plotted in Figure 5 are an indication of the relative weights of nozzles fabricated from various materials. The strength-to-weight ratios were obtained by dividing the ultimate tensile strength (UTS) by the density. These values are approximate, since the UTS can vary appreciably depending upon the method of fabrication, heat treatment, and testing techniques. In addition to the pure metals, there are many alloys of these refractory metals that could be used.

Table I. Advantages and Disadvantages of Various Wall Materials[12]

Wall Material	Advantage	Disadvantage
1. Woven Metal Cloth (Regimesh)	1. Uniform porosity.	1. Must be fabricated in conical and cylindrical shapes and welded. 2. Does not have unidirectional-radial flow. 3. Does not have large permeability variation over short distance.
2. Wound Wire (Poroloy)	1. Uniform porosity.	1. Can be constructed in only limited shapes. 2. Does not have unidirectional-radial flow. 3. Does not have large permeability variation over short distance.
3. Powdered Sintered Metal	1. Can be fabricated to desired geometrical shape.	1. Uniform porosity is not always achieved. 2. Does not have unidirectional-radial flow. 3. Does not have large permeability variation over short distance.
4. Sintered Felted Short Metal Fibers		
5. Sintered Foam Metals		
6. Photoetched Washers	1. Controlled porosity. 2. Accurate flow distribution. 3. Permeability only in radial flow direction. 4. Flexibility in choice of materials, flow patterns and washer thickness. 5. Capability of replacing individual washers or washer sections.	1. Weight 2. Initial cost will be high. 3. Close tolerances complicate fabrication.

Table II. Properties of Some Refractory Materials[13]

Property	Tungsten	Tantalum	Molybdenum	Columbium (Niobium)	Graphite
Theoretical density at 70°F, lb/in.^{3}	0.697	0.600	0.368	0.309	0.082
Melting point, °F	6170	5430	4750	4380	6600 (sublimes)
Boiling point, °F	9980	9810	8730	8910	—
Linear coefficient of thermal expansion/°C	4.3×10^{-6}	6.5×10^{-6}	4.9×10^{-6}	7.2×10^{-6}	2 to 6×10^{-6}
Specific heat at 70°F, Btu/lb-°F	0.032	0.036	0.061	0.065	0.18
Thermal conductivity, Btu-ft/hr-ft^2-°F					
Room temp	97	31	92	31	50 to 90
1000°F	80	37	75	—	40 to 80
1500°F	70	40	65	—	30 to 60
2000°F	65	42	56	—	20 to 50
2500°F	63	43	46	—	20 to 50
3000°F	61	44	39	—	20 to 40
Tensile strength, 1000 psi					
Room temp	100 to 500	100 to 150	120	75 to 150	1 to 3
1000°F	180	35	45	30	1 to 3
1500°F	—	25	35	17	1 to 3
2000°F	50	15	25	10	1 to 3
2500°F			10	4	1.5 to 4
3000°F			9		1.5 to 4.5
Young's modulus, 10^6 psi at Room temp	59	27	46	12 to 15	1 to 3

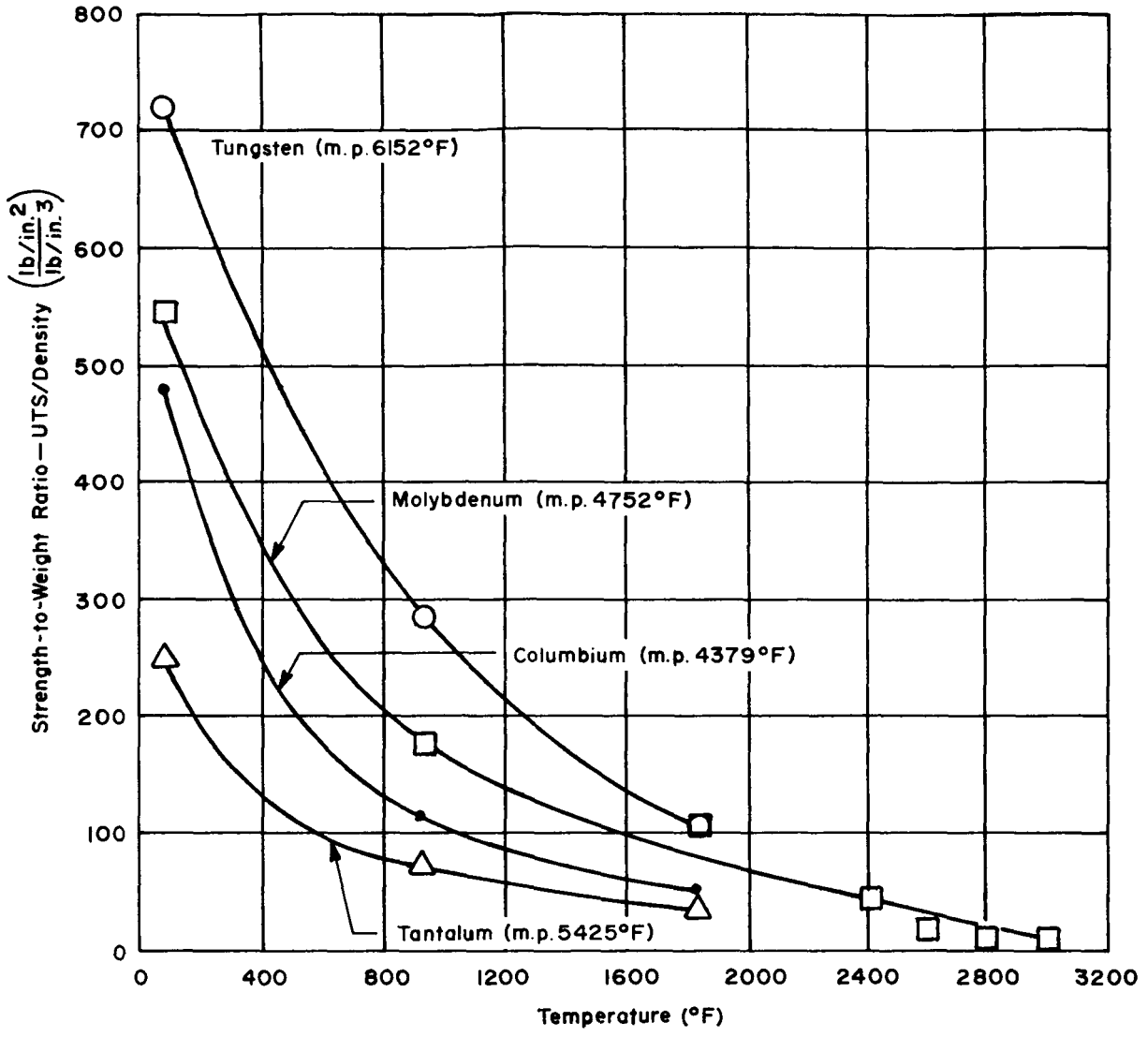

Figure 5. Strength-to-Weight Ratios of Some Refractory Metals[8]

b. Coolants

To date, most of the interest in transpiration coolants has been centered around low molecular-weight gases and liquid metals. Gases exhibit a large heat transfer reduction in both turbulent and laminar boundary layers which is a desirable property. One disadvantage in using gases, however, is the corresponding decrease in matrix thermal conductivity that results from the characteristically low conductivity of the gaseous fluid. Liquid metals offer the greatest conductivity of cooling fluids. Coolants other than gases and liquid metals have not received a great deal of attention because of the complexity of injection through the porous matrix, chemical incompatibility with the matrix, etc.[14]

Figure 6 gives the heat absorption capabilities of several transpiration coolants at 34 atmospheres of pressure. In each case, except cryogenic hydrogen, the initial temperature has been taken at 77°F. In the absence of phase change and chemical reaction, each of these curves would be nearly a straight line with a slope equal to the heat capacity of the vapor in question. Phase changes introduce the vertical jumps shown in this figure, and dissociation ($2NH_3 \rightarrow N_2 + 3H_2$) accounts for the strong upward curvature displayed by ammonia.[15]

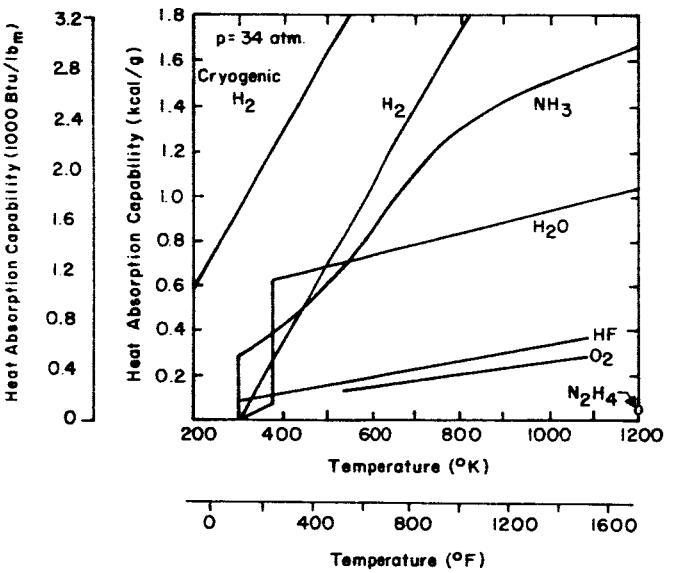

Figure 6. Heat Absorption Capabilities of Some Transpiration Coolants

The ultimate criterion for evaluating coolants is minimization of the system weight required to maintain the nozzle wall at the desired temperature. In addition, the following characteristics are desirable in coolants:[13]

1) A low m. p. and high boiling point for liquid coolants.
2) Thermal stability and compatibility with the wall material so that no reactions occur which may impair the integrity of the nozzle or interfere with the flow of the coolant.
3) Use of the coolant should not entail any complex storage, handling, or inherent safety hazards since these tend to complicate logistics and increase system weights. These considerations refer to such things as the necessity for cryogenic or pressurized storage facilities, preheating systems, and safety hazards which arise from the explosiveness or toxic nature of the coolant.

4) High storage density is desirable in order to minimize storage tank volume and weight.
5) A low molecular weight is desirable since the coolant is injected into the exhaust gas stream.
6) Knowledge of the physical properties of the fluid is necessary for proper evaluation of coolants and design of the cooling system.

Figure 7 gives the coolant weights required to maintain the wall at specified temperatures for some coolants.[13] These weights were obtained from a steady-state heat balance without consideration to the actual heat transfer mechanism, and are based on the following assumptions:

1) The heat flux to the wall remained constant at 10 Btu/sec-in.^{2}
2) The coolant was heated from the liquid at the m. p. (or gas at the boiling point for H_2, He, and N_2) to the indicated wall temperature.
3) The liquids were vaporized at an assumed nozzle pressure of 500 psia (i.e., when the coolant temperature reached the saturation temperature at 500 psia it boiled, absorbing its latent heat).

The comparative standing of the coolants depends upon the allowable wall temperature. At temperatures of about 2700°to 3500°F, lithium is the best coolant because of its high specific heat and latent heat of vaporization. Hydrogen follows closely at these high temperatures and is superior to all of the coolants, including lithium, at wall temperatures below about 2700°F. Water ranks second to hydrogen at wall temperatures below 1500°F.

c. Single-Phase Transpiration Cooling

Most of the analytical and experimental investigations on transpiration cooling have been concerned with the laminar boundary layer. This is primarily a result of the laminar flow problem being more amenable to analytical treatment than the turbulent flow. Unfortunately, transpiration cooling is more likely to be used where turbulent flow and consequently higher heating rates are involved. Even if the flow is laminar initially, the disturbance resulting from the injection of the coolant tends to cause transition to turbulent flow.[16]

The basic mechanism of heat transfer in transpiration cooling can best be understood by referring to Figure 8. The element considered has a plane surface ① coinciding with the outside wall surface, and a

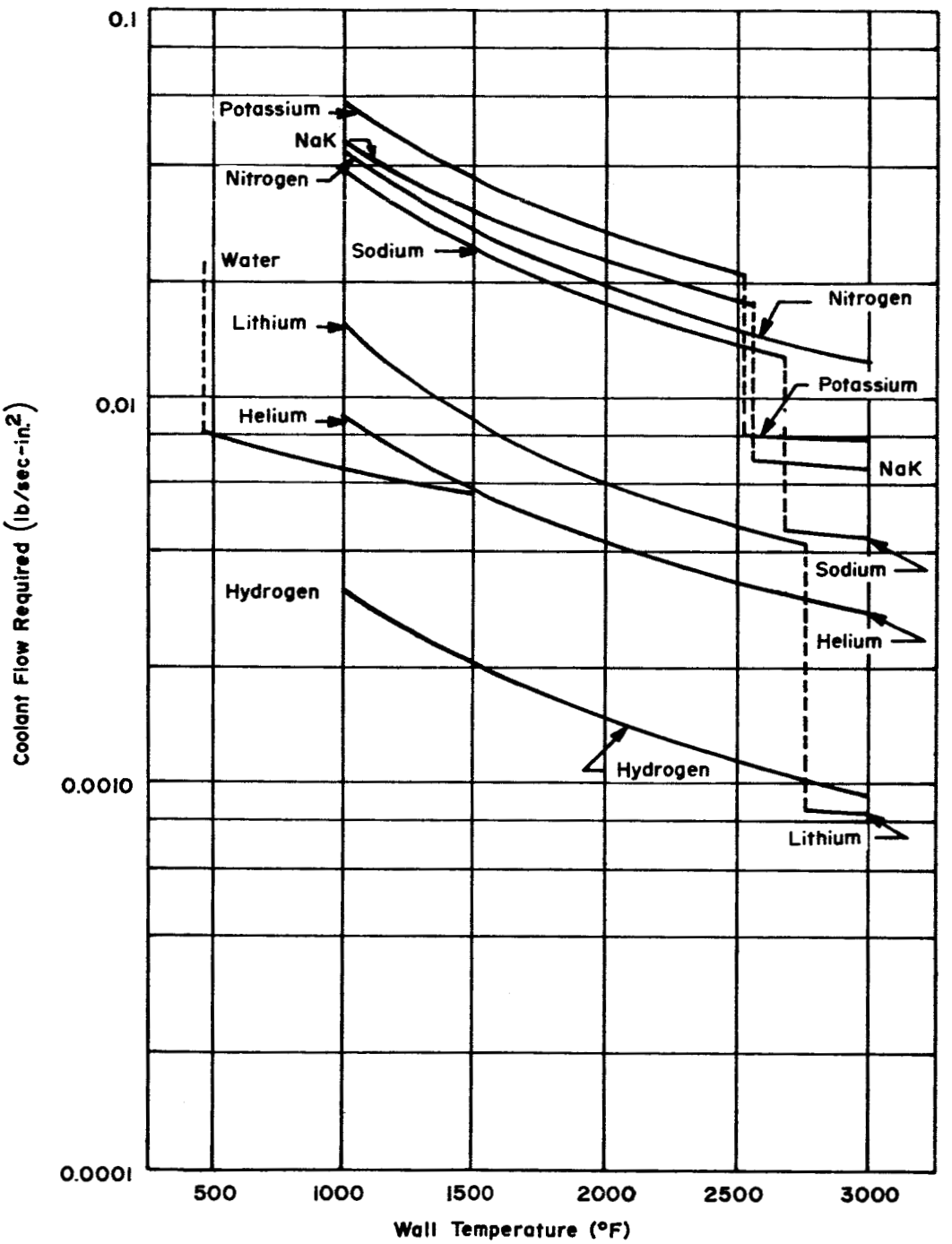

Figure 7. Coolant Weight Requirements Versus Wall Temperature

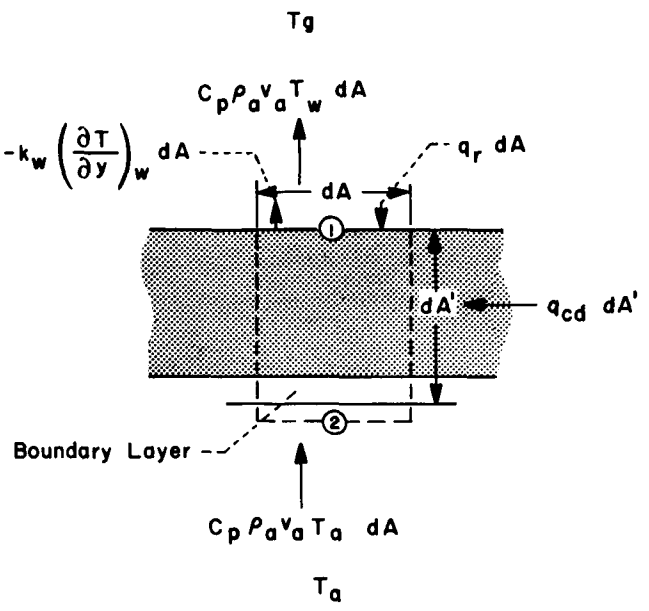

Figure 8. Sketch of Element of Wall Used in Setting Up Heat Balance for Transpiration Cooling

plane surface ② apart from the inside surface of the wall by such a distance that it is situated outside the boundary layer present on this side. Heat is carried by convection with the coolant through surfaces ① and ② . It is assumed that the coolant has attained the wall surface temperature T_w when it leaves the wall. Heat will also be transferred by conduction through the fluid layers immediately adjacent to the outside wall surface in the amount of $-k_w \left(\frac{\partial T}{\partial y}\right)_w$ dA. Furthermore, heat may be transferred to the outside wall by radiation $q_r dA$. In addition, heat may also flow into the element by conduction in the porous material or by transverse flow of the coolant within the boundary layer; the sum of these flows is designated $q_{cd} dA'$. The heat balance may then be written:

$$k_w \left(\frac{\partial T}{\partial y}\right)_w dA + q_r dA + q_{cd} dA' = c_p \rho_a v_a \left(T_w - T_a\right) dA \qquad (1)$$

For constant wall temperature and negligible heat flow along the boundary layer, $q_{cd} = 0$. If the heat transferred to the outer surface by both conduction through the fluid layers and radiation is written in terms of heat transfer coefficients, Equation (1) reduces to:

$$\frac{T_w - T_a}{T_g - T_a} = \frac{1}{1 + \frac{c_p \rho_a v_a}{\bar{h}_{g,cv}} \left(\frac{1}{\frac{\bar{h}_{g,t}}{\bar{h}_{g,cv}} + \frac{\bar{h}_r}{\bar{h}_{g,cv}}} \right)} \qquad (2)$$

The values of the heat transfer coefficients to be used in Equation (2) depend upon whether the boundary layer is laminar or turbulent. The average heat transfer coefficient may be written:

$$\bar{h}_{g,t} = c_p \rho_g V_g \overline{St}_{g,t} \tag{3}$$

The final equations for the temperature ratio, or cooling effectiveness, are given below. (Derivation of these equations is given in Report No. NACA TR 1182.[17])

1) Laminar flow without radiation ($\bar{h}_r = 0$):

$$\frac{T_w - T_a}{T_g - T_a} = \frac{1}{1 + \dfrac{\rho_a v_a}{\rho_g V_g} \dfrac{\bar{h}_{g,cv}}{\bar{h}_{g,t}} \dfrac{\sqrt{Re_g} Pr_g^{2/3}}{0.664}} \tag{4}$$

2) Laminar flow with radiation:

$$\frac{T_w - T_a}{T_g - T_a} = \frac{1}{1 + \dfrac{\rho_a v_a}{\rho_g V_g} \dfrac{\sqrt{Re_g} Pr_g^{2/3}}{0.664} \left(\dfrac{1}{\dfrac{\bar{h}_{g,t}}{\bar{h}_{g,cv}} + \dfrac{\bar{h}_r}{\bar{h}_{g,cv}}} \right)} \tag{5}$$

3) Turbulent flow without radiation:

$$\frac{T_w - T_a}{T_g - T_a} = \frac{1}{1 + \dfrac{Re_g^{0.1}}{2.11} \left(e^{r\phi} - 1 \right)} \tag{6}$$

where

$$r\phi = \frac{2.11}{0.037} Re_g^{0.1} Pr_g^{2/3} \frac{\rho_a v_a}{\rho_g V_g}$$

4) Turbulent flow with radiation:

$$\frac{T_w - T_a}{T_g - T_a} = \frac{1}{1 + \dfrac{\rho_a v_a}{\rho_g V_g} \dfrac{Re_g^{0.2} Pr_g^{2/3}}{0.037} \left(\dfrac{1}{\dfrac{\bar{h}_r}{\bar{h}_{g,cv}} + \dfrac{r\phi}{e^{r\phi} - 1}} \right)} \tag{7}$$

A comparison of transpiration cooling with convection cooling for both laminar and turbulent flow for a Prandtl number of 0.7 is shown in Figure 9. Low values of the temperature difference ratio indicate good cooling effectiveness. [17]

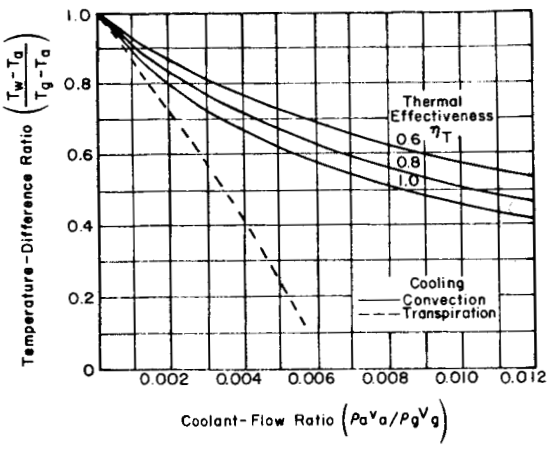

(a) Laminar flow without radiation
Reynolds number = 10^4

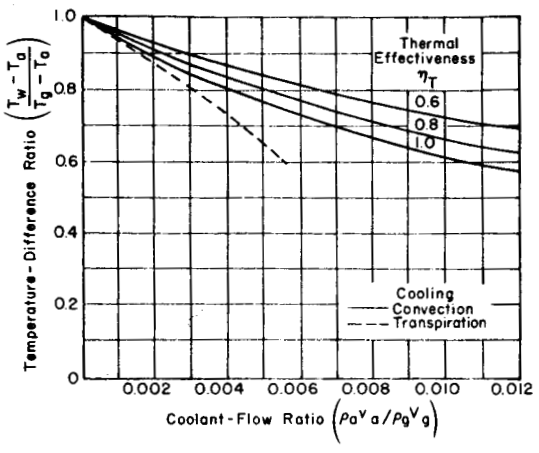

(b) Laminar flow with radiation
Reynolds number = 10^4

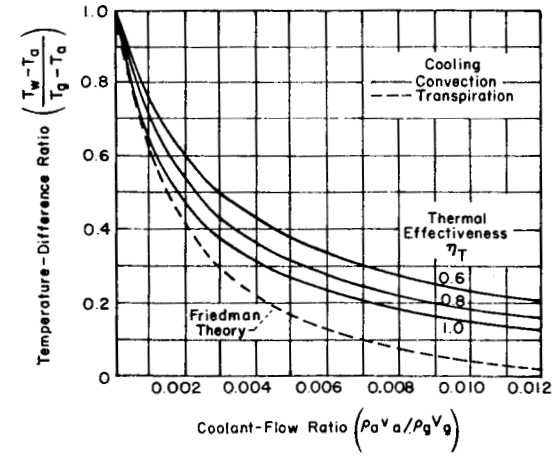

(c) Turbulent flow without radiation
Reynolds number = 10^7

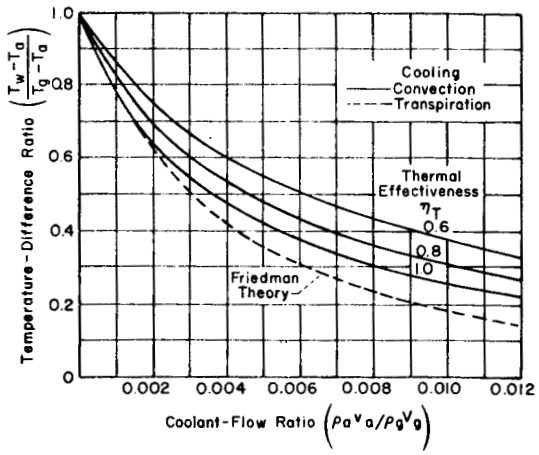

(d) Turbulent flow with radiation
Reynolds number = 10^7

Figure 9. Comparison of Transpiration Cooling with Convection Cooling[17]

A number of experimental results are reported for air injection into a turbulent boundary layer on zero pressure gradient surfaces.[18, 19, 20, 21, 22, 23] Figure 10 compares the available heat transfer results in the form of Stanton numbers with several analyses. The three analyses do not differ markedly, although Dorrance and Dore[24] are somewhat lower. The experimental data, covering a range of Mach numbers from 0 to 2.7 show considerable scatter, but the trend is correctly predicted by all three analyses. Similar results for skin friction are shown in Figure 11, and the bulk of the data tends to agree with the prediction of Rubesin and van Driest. The only conflicting evidence is the experimental data of Mickley and Davis[23] which show skin-friction values much lower than the other investigators -- even lower than those predicted by the film theory. Since the majority of the experimental data favors Rubesin and van Driest, it appears that this represents the more realistic and certainly the more conservative estimate of skin friction and heat transfer in the presence of air injection.

To determine the influence of molecular weight of the coolant gas on the heat transfer and skin friction, the mass transfer parameter was plotted against the molecular weight at a constant value of the reduced parameter, C_f/C_{f_o} and C_H/C_{H_o} of 0.5. The results are shown in Figure 12 where it is seen that the molecular weight plays a more significant role for the light gases, while the heavier gases do not appear to be so sensitive to this property.[25]

Librizzi and Cresci[1] investigated experimentally the downstream influence of mass injection on the heat transfer to the surface of an axisymmetric nozzle in turbulent flow. Helium and nitrogen were used as coolants and were injected through a porous region upstream of the nozzle throat at various rates. The results of the experiments showed a decrease in heat transfer with increasing mass injection, helium being more effective for the same mass flow rate than nitrogen. This decrease in heat transfer became less prominent as the distance downstream of the porous region increased.

Bernicker[8] studied transpiration cooling of a two-dimensional nozzle with relatively low test pressures resulting in a laminar boundary layer. Two test nozzles were used, each having the porous region at a different position with respect to the nozzle throat. Helium and air were used as coolants. The results showed an appreciable decrease in the equilibrium surface temperature over the zero injection case, with the decrease due to helium injection persisting for a greater distance downstream of the injection area.

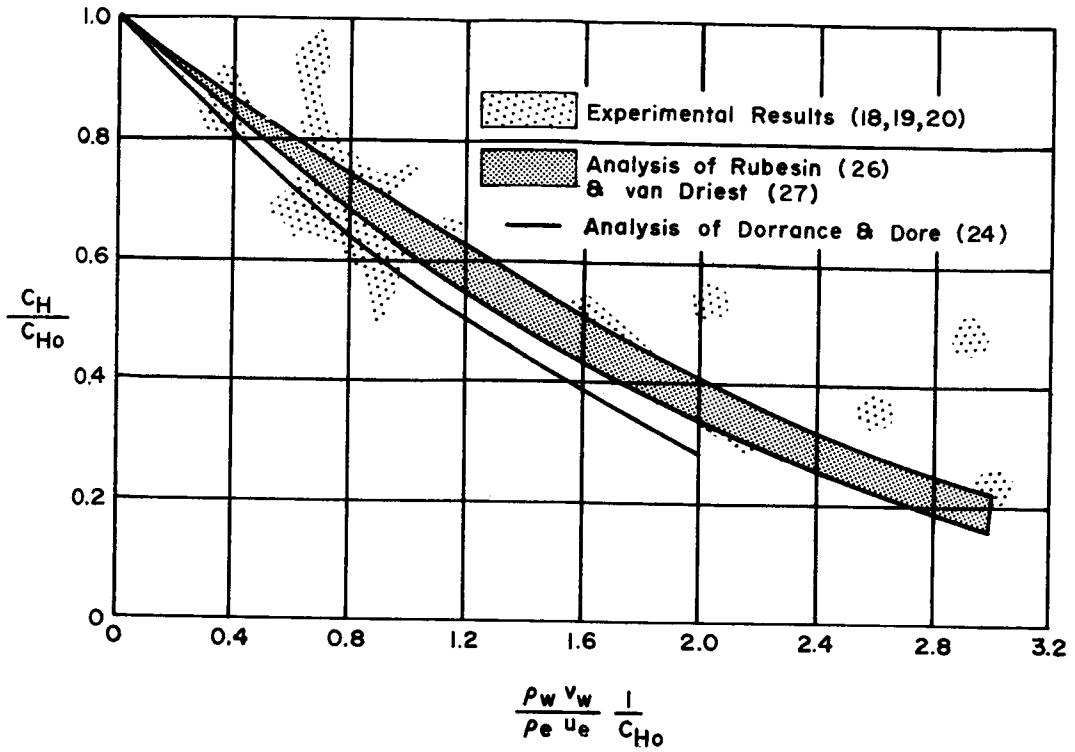

Figure 10. Comparison of Heat Transfer Results

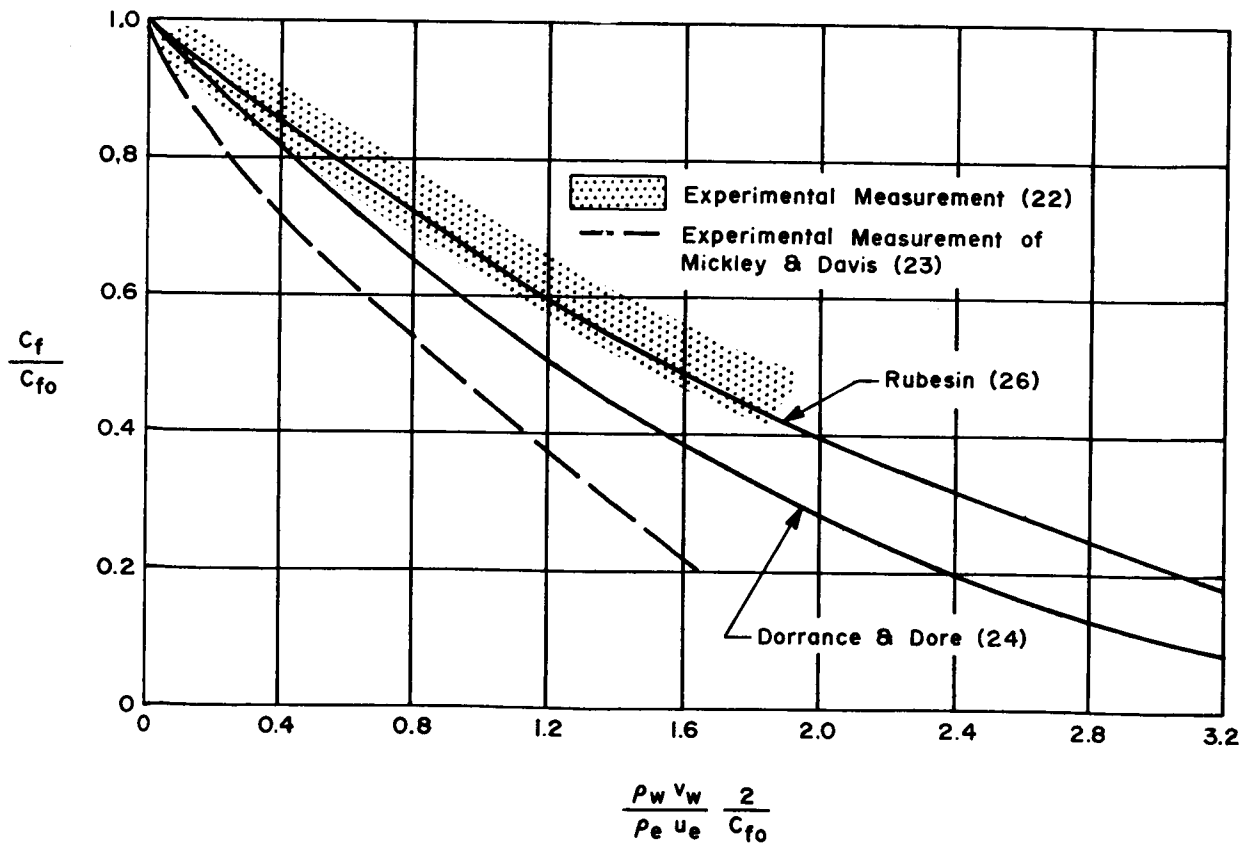

Figure 11. Predicted and Measured Skin Friction for Air Injection into a Turbulent Boundary Layer

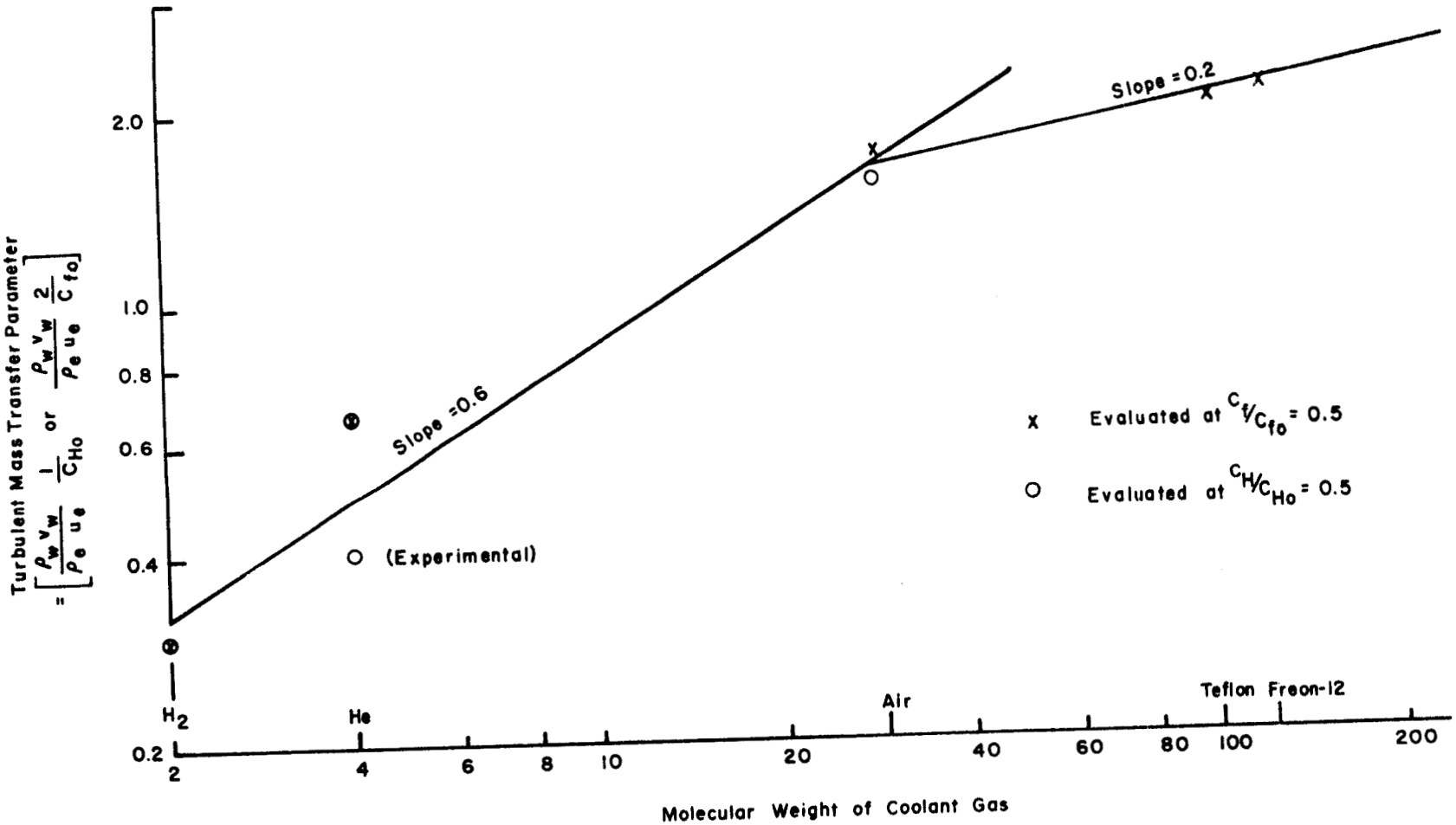

Figure 12. Turbulent Mass Transfer Parameter Versus Molecular Weight of Coolant Gas

d. Two-Phase Transpiration Cooling[8]

A review of the literature reveals that very little experimental work has been done in two-phase transpiration cooling. There are several advantages which two-phase transpiration cooling provides. As with evaporative film cooling, full use is made of the coolant's latent heat of vaporization. In addition, when vaporization of the coolant takes place within the wall structure, the heat capacity of the superheated vapor also contributes to the cooling effect.

A sketch of the model portraying the two-phase process is shown in Figure 13. The liquid is heated to saturation temperature in Region II, and in Region III boiling occurs at constant temperature. The

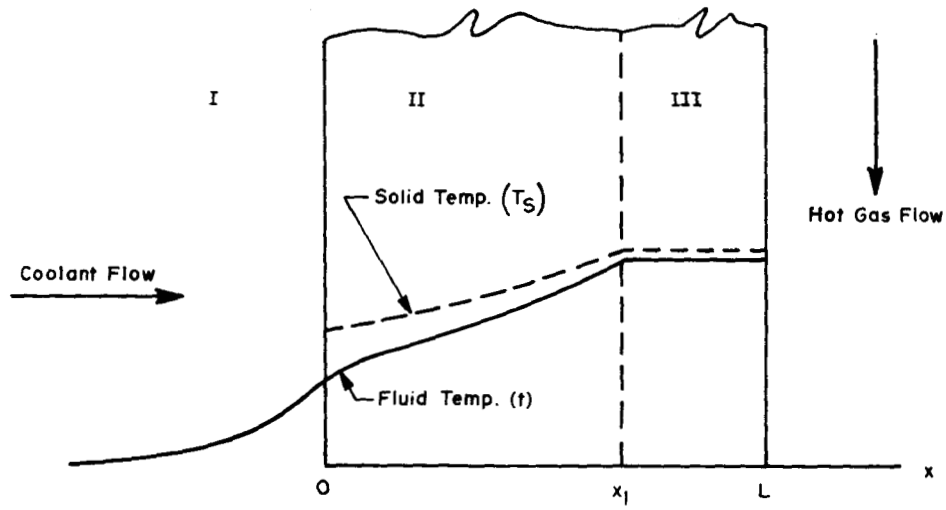

Figure 13. Two-Phase Coolant System (Coolant Exits at a Quality)[13]

assumption was made that inside the wall $T_s \geq t$ and $dt_s/dx \geq 0$. Since boiling occurs at constant temperature in Region III:

$$\left(\frac{dt}{dx}\right)_{III} = 0 \tag{8}$$

If it is also true that at $x = L$, $T_s = t$ and $x \leq L$, $T_s \geq t$ and $dT_s/dx \geq 0$, the following statement must also be true:

$$\left(\frac{dT_s}{dx}\right)_{III} = 0 \tag{9}$$

The combination of Equations (8) and (9) represents a zero heat flux in Region III. There are two solutions possible.

(1) $L - x_1 \approx 0$. In this case, the liquid is actually exiting from the pores at saturation temperature and is boiling at the boundary x = L. It is then possible to have a finite solid temperature gradient x = L.

(2) $T_s \neq t$ at x = L. It is then possible for:

$$\left(\frac{dT_s}{dx}\right)_{x=L} > 0. \tag{10}$$

The fluid in the first solution can be treated as a single phase throughout. The temperature distribution in the wall can be obtained from the analysis of single-phase flow. The possibility of boiling occurring at the boundary is, of course, dependent on the heat transfer in the boundary layer.

The second solution can be handled analytically, since boundary condition can be found to replace $T_s = t$ at x = L. The mathematical description of Region II is the same as that given in the single-phase case with the suitable substitution of the system properties.

Region II

$$T_s = C_0 + \sum_{n=1}^{3} k_n C_n e^{\lambda_n x} \tag{11}$$

$$t = C_0 + \sum_{n=1}^{3} C_n e^{\lambda_n x} \tag{12}$$

In Region III, the heat balance for the solid is characterized by:

$$(1 - \epsilon) k_\omega \frac{d^2 T_s}{dx^2} = ha\,(T_s - t_s) \tag{13}$$

Equation (13), when integrated, becomes:

$$T_s = t_{st} B_1 e^{\delta x} + B_2 e^{-\delta x} \tag{14}$$

Since the boiling temperature is assumed constant, the energy balance for the fluid phase involves the enthalpy:

$$G\frac{dH}{dx} = ha(T_s - t_s) \tag{15}$$

Substituting Equation (14) into Equation (15) and integrating yields the enthalpy distribution in the boiling region:

$$H = B_0 + \frac{\Omega}{\delta} B_1 e^{\delta x} - \frac{\Omega}{\delta} B_2 e^{-\delta x} \tag{16}$$

Equations (11), (12), (14), and (16) represent the solution to the temperature profile in the porous wall. The boundary conditions needed to evaluate the seven constants of integration and the location of x_1 are:

At $x = L$

1) $H = H_2$

2) $(1 - \epsilon)\, k_\omega \left(\frac{dT_s}{dx}\right) = G\left[C_{pL}\left(t_s - t_R\right) + \left(H_2 - H_1\right)\right]$

At $x = x_1$

3) $H = H_1$

4) $T_{sII} = T_{sIII}$

5) $t_{II} = t_s$

6) $(1 - \epsilon)\, k_\omega \left(\frac{dT_s}{dx}\right)_{II} + \epsilon k_L \left(\frac{dt}{dx}\right)_{II} = GC_{pL}\left(t_s - t_R\right)$

7) $\left(\frac{dt}{dx}\right)_{II} = 0$

At $x = o$

8) $\left(\frac{dT_s}{dx}\right)_{II} = 0$

Figure 14 shows a model where the coolant is heated to boiling temperature in Region II and boils at constant temperature in Region III, and the vapor is superheated in Region IV. In Regions II and IV, the general solution to the temperature profiles is similar to that given in the single-phase analysis.

Region II

$$T_s = E_0 + \sum_{n=1}^{3} L_n E_n e^{\nu_n x} \tag{17}$$

$$t = E_0 + \sum_{n=1}^{3} E_n e^{\nu_n x} \tag{18}$$

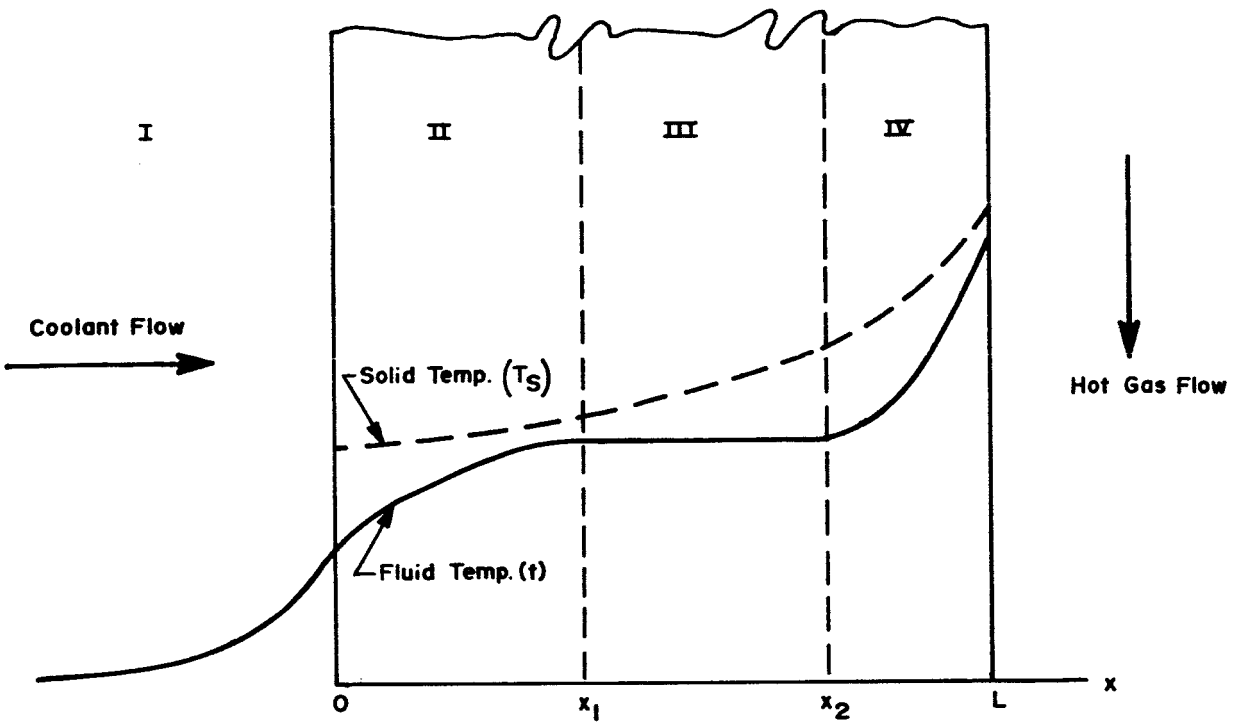

Figure 14. Two-Phase Coolant System (Coolant Exits Superheated) [13]

Region III

$$T_S = t_S + B_1 e^{\delta x} + B_2 e^{-\delta x} \tag{19}$$

$$H = B_0 + \frac{\Omega}{\delta} B_1 e^{\delta x} - \frac{\Omega}{\delta} B_2 e^{-\delta x} \tag{20}$$

Region IV

$$T_S = F_0 + \sum_{n=1}^{3} P_n F_n e^{\lambda_n x} \tag{21}$$

$$t = F_0 + \sum_{n=1}^{3} F_n e^{\lambda_n x} \tag{22}$$

The boundary conditions needed to evaluate the 11 constants of integration and the location of the boiling region are:

At $x = L$

1) $t = t_L$

2) $(1 - \epsilon)\, k_\omega \frac{dT_s}{dx} + \epsilon k_v \frac{dt}{dx} = G\left[C_{pL}(t_s - t_R) + (H_2 - H_1) + C_{pL}(t_L - t_s)\right]$

At $x = x_2$

3) $H = H_2$

4) $t_{IV} = t_s$

5) $T_{sIII} = T_{sIV}$

6) $\left(\frac{dt}{dx}\right)_{IV} = 0$

7) $(1 - \epsilon)\, k_\omega \left[\frac{dT_s}{dx}\right]_{III} = G\left[C_{pL}(t_s - t_R) + (H_2 - H_1)\right]$

At $x = x_1$

8) $H = H_1$

9) $t_{II} = t_s$

10) $T_{sII} = T_{sIII}$

11) $\left[\frac{dt}{dx}\right]_{II} = 0$

12) $(1 - \epsilon)\, k_\omega \left[\frac{dT_s}{dx}\right]_{II} + \epsilon k_L \left[\frac{dt}{dx}\right]_{II} = GC_p(t_s - t_R)$

At $x = o$

13) $\frac{dT_s}{dx} = 0$

The United Nuclear Corporation conducted some experimental work[13] on two-phase transpiration cooling. The experiment was not intended to simulate rocket nozzle conditions, but was simply designated to demonstrate this method of cooling and compare transpiration cooling with water and nitrogen.

Initial experiments were performed with the low density, woven, type 304 stainless "Rigimesh" specimen made by Aircraft Porous Media, Incorporated. The specimen was 2 inches by 2 inches by 1/8 inch thick.

The temperature on both faces of the specimen was measured by thermocouples. Both nitrogen and water, as coolants, were passed in the specimens, while the hot gas temperature was in excess of 2000°F. With no coolant, the hot-gas side reached 1400°F. Outside wall temperatures of 400°to 800°F were measured with nitrogen flows of 0.6 to 2.4 ft^3/min, and 220°F with a water flow of about 5.6×10^{-4} ft^3/min. The results of this experiment are summarized in Tables III and IV.

Double wall specimens consisting of two $1/8$-inch thick sections of grade "X" sintered stainless steel made by Aircraft Porous Media, Incorporated were also used. These specimens became partially plugged with impurities from the water. A filter with pores smaller than those in the specimen should be used. Nevertheless, two-phase flow in a porous wall was demonstrated.

Table III. "Rigimesh" Specimen with Nitrogen Coolant

Run	Outside Wall Temp. °F	Inside Wall Temp. °F	Hot Gas Temp. °F	Nitrogen Flow ft^3/min	Heat Flux Btu/sec-in.^{2}
1	1250	545	>2000	1.84	0.21
2	1005	415	>2000	2.40	0.21
3	1080	550	>2000	1.31	0.12
4	1235	780	>2000	0.64	0.071
5	1285	822	>2000	0.64	0.075

Table IV. "Rigimesh" Specimen with Water Coolant

Run	Inside Wall Temp. °F	Hot Gas Temp. °F	Water Flow, ft^3/min	Comments
1	220	>2000	7.4×10^{-4}	Excess water at bottom of porous wall.
2	225	>2000	4.4×10^{-4}	Porous wall wetted to mid-plane.
3	812→680	>2000	3.0×10^{-4}	Only bottom $1/8$ in. of wall wetted.
4	220	>2000	5.6×10^{-4}	Entire wall just wetted with no excess water.

3. Self-Cooling

The self-cooling process (Figure 3) can be described in the following manner: after ignition, the temperature of the surface rises rapidly until the coolant melts and then flows through the matrix under the action of pressure forces; all fluid emerging from the hot surface is vaporized resulting in a gaseous-liquid coolant interface that recedes with time; the rate of recession of the interface and, consequently, the gaseous coolant mass flow rate are functions of the temperature distribution within the composite and of the pressure drop through the porous structure caused by viscous and inertial effects on the coolant mass flow; the vaporization of the coolant and interface recession will continue until firing is terminated or the coolant is exhausted. The following cooling mechanisms are possible in the process:

1) Heat absorption at the gaseous-liquid interface where the coolant vaporizes.
2) Convective cooling as the gaseous coolant flows through the porous structure.
3) Reduction of the convective heat transfer coefficient by mass addition into the boundary layer (transpiration cooling effect).
4) Heat absorption within the composite if the gaseous coolant dissociates internally.
5) Heat absorption at the surface if an endothermic reaction takes place between the gaseous coolant and hot gas.

In addition to these mechanisms, chemical reactions may occur that are unfavorable from the standpoint of heat transfer. It is possible that dissociated products may recombine in the vicinity of the surface to cause severe heating. Exothermic chemical reactions between the coolant and the hot gas would also have an unfavorable effect on heat transfer.[28]

Despite the interest in the self-cooling concept, very few theoretical analyses have been developed. The analysis which appears to be the most prevalent is that of Gessner et al.[29] These investigators considered the flow of hot gas through a rocket nozzle having a throat insert consisting of a porous refractory matrix, which is filled with an infiltrant (Figure 15). If the thickness of the insert is small compared to the nozzle-throat radius, the insert can be considered to be an infinite plate of finite thickness. The plate is considered to be a tungsten-infiltrant composite of constant porosity with a single infiltrant that vaporizes below the melting point of the refractory matrix. After the surface is heated and the infiltrant boiling point is reached, a

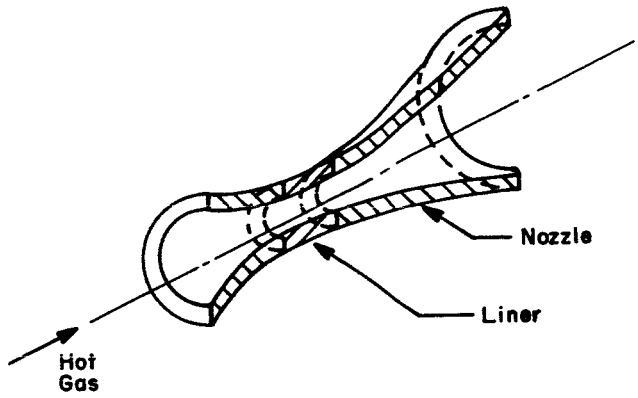

Figure 15. Flow of Hot Gas Through a Rocket Nozzle with a Liner at the Throat [29]

liquid/vapor interface begins to recede and infiltrant vapor starts to flow through the porous structure. A schematic diagram of the model after heating has begun and the liquid/vapor interface has formed is shown in Figure 16. Recession of the liquid/vapor interface continues until heating is ended or until the infiltrant is exhausted. To simplify the analysis, the following conditions were prescribed:

1) One-dimensional, unsteady-state heat transfer.
2) Temperature-constant thermophysical properties.
3) Equal matrix and infiltrant vapor temperatures at a given depth in the porous structure.
4) Heat of fusion of infiltrant combined with heat of vaporization.
5) Negligible heat conducted through infiltrant in gaseous phase as compared to heat conducted through the porous matrix.
6) Negligible radiation between hot gas and heated surface as compared to convective heating.
7) No diffusion or chemical reactions between infiltrant vapor and hot gas.
8) Negligible radiation within porous structure.

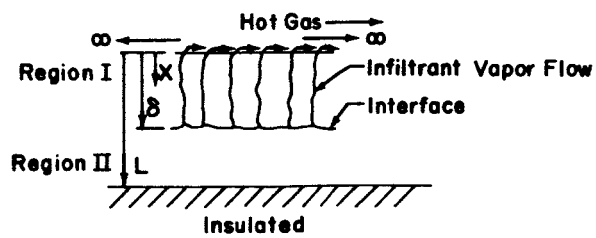

Figure 16. Model After the Liquid/Vapor Interface Has Formed [28]

After heating has begun, but before vaporization of the infiltrant occurs, a heat balance of any internal volume element can be written:

$$\left|k_m(1 - P) + k_c P\right| \frac{\partial^2 T}{\partial x^2} = \left|\rho_m C_m (1 - P) + \rho_c C_c P\right| \frac{\partial T}{\partial \theta} \tag{23}$$

where

$$T = T(x, \theta)$$

The corresponding initial condition and boundary conditions are written:

$$T(x, 0) = T_0 \tag{24}$$

$$-\left|k_m(1 - P) + k_c P\right| \left(\frac{\partial T}{\partial x}\right)_{x=0} = h_0 (T_g - T)_{x=0} \tag{25}$$

$$(0 < \theta < \theta_1)$$

$$\left(\frac{\partial T}{\partial x}\right)_{x=L} = 0 \qquad (0 < \theta < \theta_1) \tag{26}$$

After vaporization occurs and a liquid/vapor interface forms, two regions exist for which heat balances must be written. The first region is between the heated surface and the interface, and the second is between the interface and the insulated surface. The heat balances and corresponding initial and boundary conditions can be written:

Region 1 = between heated surface and liquid/vapor interface:

$$0 \le x \le \delta$$

$$k_m(1 - P) \frac{\partial^2 T}{\partial x^2} + \left(C_c\right)_g \left(G_c\right)_g \frac{\partial T}{\partial x} = \rho_m C_m (1 - P) \frac{\partial T}{\partial \theta} \tag{27}$$

with

$$-k_m(1 - P) \left(\frac{\partial T}{\partial x}\right)_{x=0} = h(T_g - T) \tag{28}$$

$$(\theta_1 \le \theta \le \theta_{max})$$

$$-k_m(1 - P)\left(\frac{\partial T}{\partial x}\right)_{\delta^-} = (G_c)_g \lambda_v - \left|k_m(1 - P) + k_c P\right|\left(\frac{\partial T}{\partial x}\right)_{\delta+} \qquad (29)$$

$(0_1 \leq \theta \leq \theta_{max})$

Region 2 = between liquid/vapor interface and insulated surface:

$\delta < x \leq L$

$$\left|k_m(1 - P) + k_c P\right|\frac{\partial^2 T}{\partial x^2} = \left|\rho_m C_m(1 - P) + \rho_c C_c P\right|\frac{\partial T}{\partial \theta} \qquad (30)$$

with Equation (29) applicable at the interface with

$$\left(\frac{\partial T}{\partial x}\right)_{x=L} = 0 \qquad (\theta_1 \leq \theta \leq \theta_{max}) \qquad (31)$$

When heating begins, but before vaporization of the infiltrant occurs $(0 < \theta < \theta_1)$, the temperature distributions can be determined readily in closed form by Equation (23) by the separation of variables technique. At the instant the infiltrant vaporizes, however, a set of two partial differential equations [Equations (27) and (30)] must be solved which are coupled by the interface equation [Equation (29)].

Based upon the foregoing model and theory, a one-dimensional numerical solution was programmed for the IBM 7094 computer by Gessner et al. To check the accuracy of the computer solution, a comparison was made to the theoretical solution of Grosh[30] and the agreement was excellent, as may be seen in Figure 17, which is a typical case of porous tungsten infiltrated with zinc. In this figure, the interface recession is plotted against time.

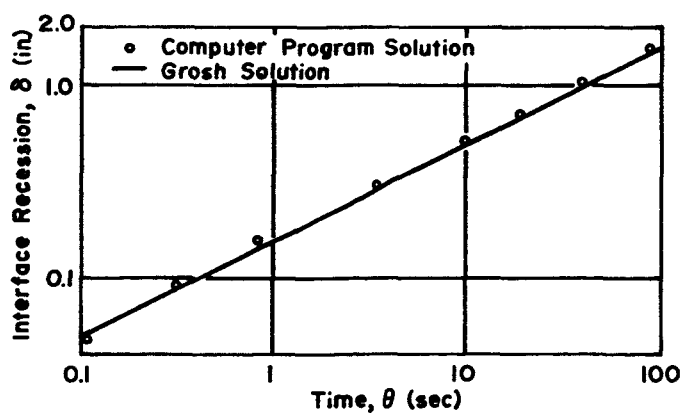

Figure 17. Comparison of Computed Interface Recession Distance with Grosh Solution: Zinc, P = 0.3

In Figure 18, the interface recession for various infiltrants is plotted against time. An explanation of this figure is as follows:

a. Teflon (Case 7)

The very low dissociation temperature (1400°F) and low thermal diffusivity of Teflon causes almost immediate recession (θ_1 = 0.25 sec). Exhaustion of the infiltrant occurred in only about 30 seconds.

b. Zinc (Case 3)

The low boiling point of zinc (2313°F) results almost in immediate interface recession also (θ_1 = 1.3 seconds). The zinc coolant was exhausted in about 72 seconds. Zinc was markedly superior to silver until the zinc was exhausted.

c. Silver (Case 1)

The beginning of recession θ_1 does not occur until 47.9 seconds because of silver's high boiling point and, to a lesser extent, the high thermal diffusivity of the composite. The high volumetric latent heat of silver results in slow interface recession.

d. Silver (Case 14)

All of the cases previously discussed were for a matrix porosity of 20 percent. Case 14 is for an 80 percent porous matrix. Recession for this case commences at about the same time as for Case 1. Increased porosity was found to reduce significantly the composite thickness requirement.

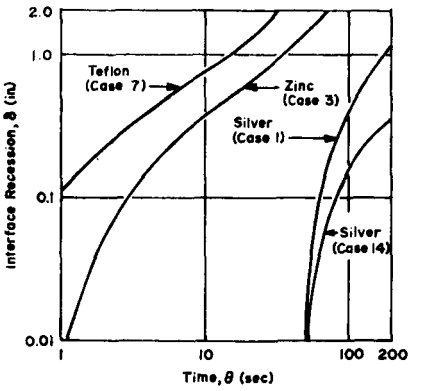

Figure 18. Interface Recession for Various Infiltrants

The general conditions under which the above experiments were conducted were typical of those encountered in a solid rocket engine with a two-inch thick insert:

Hot gas temperature	= 6200°F
Reynolds number	= 190,000
Hot gas specific heat	= 0.446 Btu/lb-°F
Hot gas mass velocity	= 1,233,000 lb/hr-ft^2
Hot gas pressure	= 226 psia
Stanton number	= 0.00237
Convective heat-transfer coefficient	≡ 1303 Btu/hr-ft^2-°F
Initial composite temperature	= 70°F

The above cases are only a sample of the experimental work performed on self-cooling. Additional data and results on other infiltrants, including ammonium chloride and lithium chloride, are available.[28]

No references to the literature could be found on any analytical or experimental work which was conducted in connection with this type of cooling to liquid rocket nozzles. Although several coolants were investigated, no definite recommendation of certain coolants over others was made. This, of course, can be easily understood since the selection of a particular coolant would depend greatly on the intended application and the particular environment such as temperature, firing time, etc., against which the nozzle is to be protected.

4. List of Symbols for Transpiration Cooling

a = Specific area per unit volume of porous wall.

A = Surface area.

A' = Surface area separating element under consideration.

c = Specific heat.

cp, Cp = Specific heat at constant pressure.

C_f = Local skin friction coefficient with mass transfer.

C_H = Local heat transfer Stanton number in presence of mass transfer.

C_{H_o} = Local heat transfer Stanton number in presence of mass transfer referring to solid wall subject to the same free stream conditions and held at same temperature as the actual wall.

e = Refers to conditions at outer edge of boundary layer.

G = Flow rate per unit area.

h = Film coefficient.

h_o = Convective heat-transfer coefficient with no transpiration.

$\bar{h}$ = Local heat transfer coefficient.

H = Enthalpy of fluid.

k = Thermal conductivity.

P = Interconnected porosity.

Pr = Prandtl number.

q = Heat flow.

Re = Reynolds number.

$\bar{St}$ = Local Stanton number.

t = Fluid temperature.

T = Temperature.

T_s = Solid temperature.

TP = Boiling.

u, v = Velocities, parallel and normal to surface, respectively.

x, y = Distance.

δ = Root of differential equation.

ϵ = Porosity.

θ = Time.

θ_1 = Time at which interface recession begins.

λn = Root of differential equation.

ν_n = Root.

ρ = Density.

$\rho_a \nu_a$ = Average mass velocity of coolant.

$\rho_g V_g$ = Average mass velocity of main flow.

$\phi = C_p \rho_a \nu_a / \bar{h}_{g,cv}$.

$\Omega = h_{TP} a/G$.

Subscripts

a = Coolant.

c = Infiltrant.

cd = Conduction.

cv = Convection.

g = Combustion gas or gas side.

L = Liquid.

m = Matrix material.

r = Radiation.

R = Reservoir.

s = Boiling point.

t = Transpiration.

w = Wall.

Section III. FILM COOLING

1. Status of Film Cooling

The film cooling technique, permitting simple thrust-chamber wall construction, was used in many early rockets, notably the German V-2 nozzle. Either liquid or gaseous coolant is injected along the gas side wall surface by means of tangential or nearly tangential coolant holes, slots, or louvers. The coolant alters the temperature profile through the thermal boundary layer, and decreases the heat flux to the nozzle wall. Where a combustion chamber of short length is used, injection can be provided at the injector face, and the film-cooling effect will persist to the throat region. In a fully film-cooled design, injection points are located at incremental distances along the wall length as shown in Figure 19 for liquid film cooling. In liquid film cooling, the vaporized film coolant does not diffuse rapidly into the main gas stream but persists as a protective mass of vapor adjacent to the wall for an appreciable distance downstream from the terminus of the liquid film. Thus the length of the hot gas flow passage protected by film cooling is significantly longer than that of the liquid film.[31]

With liquid film cooling, heat is transferred principally by means of evaporation. With gaseous film cooling, heat transfer occurs by means of sensible heat exchange. Liquid film cooling has an advantage over gaseous film cooling in that the density storage requirements are less, and the utilization of the latent heat of vaporization of a liquid significantly improves the cooling technique.[32] Generally, liquids have higher specific heats than gases although hydrogen and helium are exceptions.

Judicious spacing of injection locations can provide optimum wall-temperature distribution. Inefficient cooling results from overcooling of the wall in the injector region. Also, the large variation in wall temperature can result in severe thermal stresses. Injection velocity and injection manifold design are important because proper matching of film coolant to mainstream gas velocity can contribute to a reduction in coolant flow as a result of improved efficiency.[2]

Film cooling may be used effectively to protect the combustion chamber and nozzle walls in several ways as follows:[33]

1) Reduction of the "adiabatic" wall temperature to a value below the material limiting value.

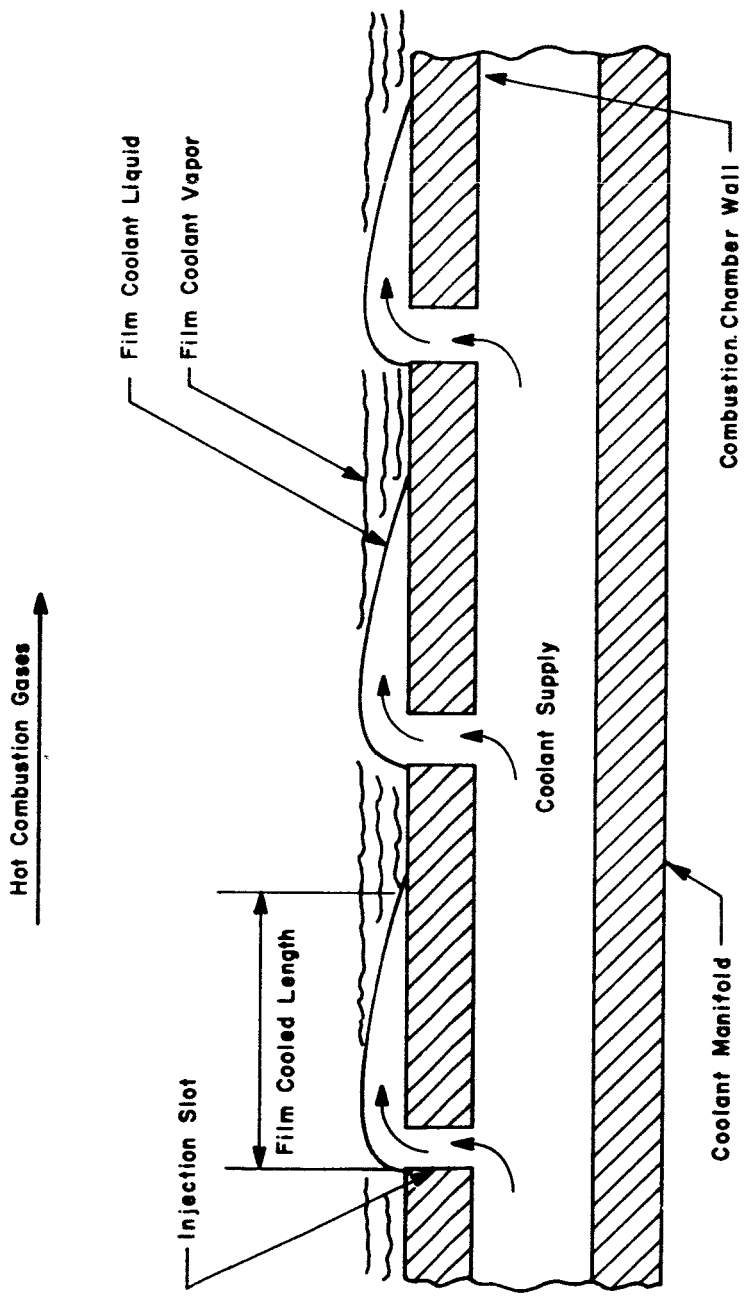

Figure 19. Film Cooled Combustion Chamber[31]

2) Reduction in the heat flux to a wall which is also cooled by radiation, convection, or a heat sink.
3) Maintaining a non-oxidizing gas adjacent to refractory surfaces otherwise capable of withstanding full combustion gas temperature, such as uncooled tungsten, tantalum, or various carbides.

With film cooling, there are no inherent limitations on cooling capacity (as found with regenerative cooling), time (as with ablative cooling), or chamber pressure (as with radiation cooling). However, a disadvantage to film-cooled design is where one of the propellants (usually the fuel) or an inert fluid is used as a coolant at the nozzle throat, there is a performance penalty (specific impulse loss) due to gas and temperature stratification.[33] The stratification loss is a variable depending upon the effective film temperature, and is independent of the effective chemical combustion efficiency. The magnitude of this effect on specific impulse is presented for various film temperatures and film thickness in Figure 20. An additional specific impulse loss may be incurred due to the operation at propellant mixture ratios other than optimum in order to insure sufficient propellant as film coolant. Film coolants such as hydrogen, helium and ammonia show promise because low molecular weight will contribute to a high ratio of temperature to molecular weight without coolant combustion, and, hence, no appreciable performance degradation will occur.[2]

If the performance loss element is taken into consideration, the most likely film-cooling applications would be either in supplementation or in large-thrust designs where only a small percentage of the total propellant flow would be required.[2]

Gaseous film cooling has been found to be an effective cooling method both analytically and experimentally, and the feasibility of this method has been established. Special attention will have to be given to the velocity ratio of coolant to free stream at the point of injection before liquid film cooling can be demonstrated with complete success.[4] Also, surface film stability under high turbulance, phase changes along the cooled length, and endothermic or exothermic decompositions are problems which require further study in liquid film cooling.[2] Although considerable analytical and experimental work has been devoted to the complex phenomenon of film instability, the results are subject to controversy and inadequately verified analytical solutions. A thorough analysis of film instability background is available.[34] Work is being devoted to developing an analytical model and applying it to experimental data on the problem of the boundary layer in liquid film cooling of rocket nozzles.[35]

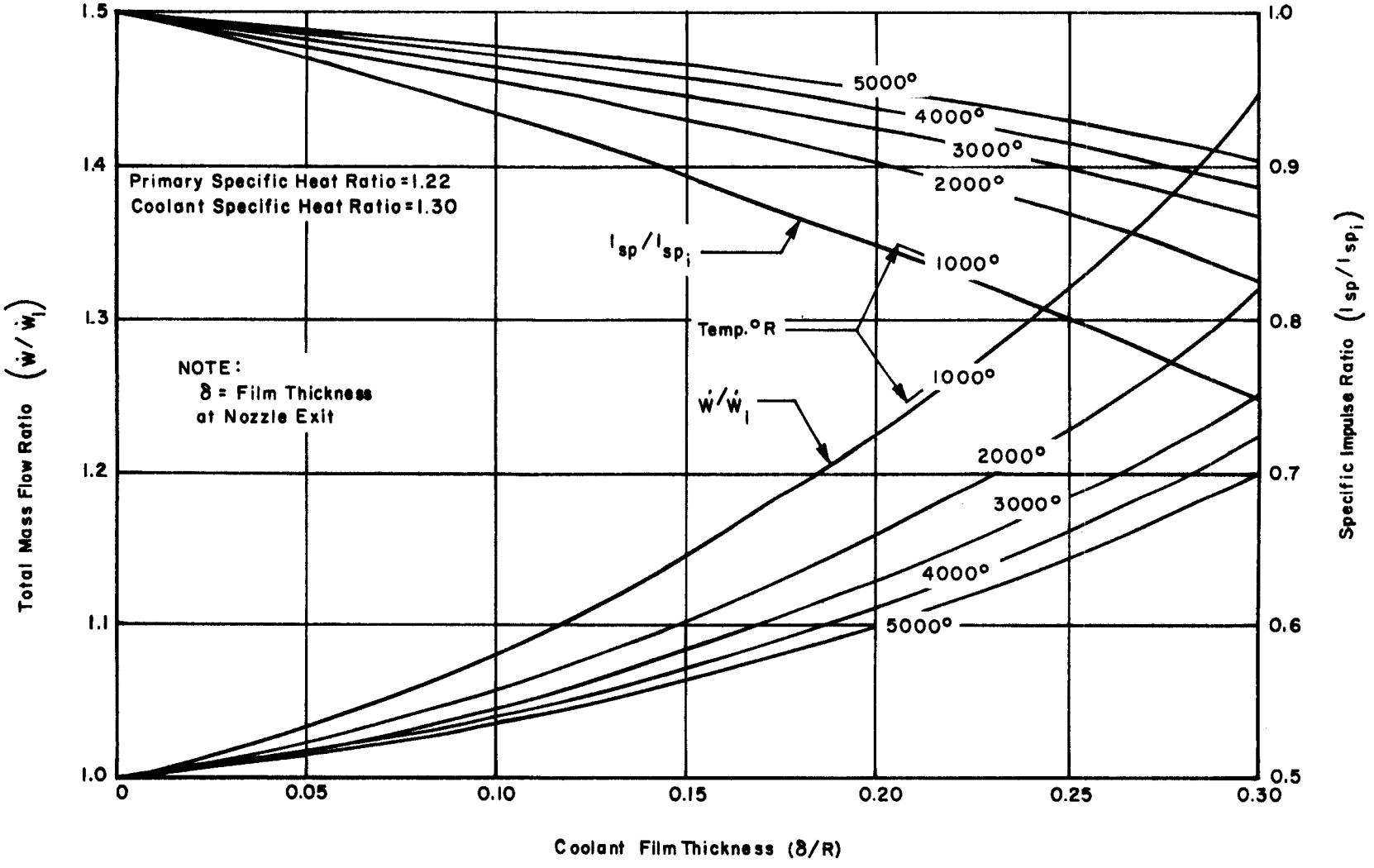

Figure 20. Rocket Engine Performance Variation with Coolant Film Thickness [33]

2. Theoretical and Experimental Investigations

a. Gaseous Film Cooling

(1) Theoretical Investigations. Several correlations of predicted adiabatic wall temperature with film cooling are available.[1,4,24,36,37,38,39,40,41,42,43,44,45,46] In many cases, analyses were empirically derived and employed to correlate experimental data obtained at relatively low temperature differences between the gas stream and the injected coolant.

The boundary-layer model of a film cooled surface has been used by many authors to derive an analytical expression for film cooling effectiveness η in terms of the Reynolds number of the cooling fluid at the slot exit $V_c y_c/\nu$, the ratio of coolant velocity to mainstream velocity V_c/V_g, and the ratio of downstream distance to slot width x/y_c, in the form[43,45]

$$\eta = \text{constant} \left(\frac{V_g x}{V_c y_c}\right)^{-0.8} \left(\frac{V_c y_c}{\nu}\right)^{0.2} \tag{32}$$

where

$$\eta = \frac{T_{ad} - T_{ad'}}{T_{ad} - T_c}$$

In early work, the following expressions were deduced by Wiegardt[38] (assuming that the boundary-layer thickness equals $0.37 \times \left(Vx/\nu\right)^{-1.2}$):

$$\eta = 5.44 \left(\frac{V_g x}{V_c y_c}\right)^{-0.8} \left(\frac{V_c y_c}{\nu}\right)^{0.2} \tag{33}$$

Tribus and Klein:[41]

$$\eta = 4.62 \left(\frac{V_g x}{V_c y_c}\right)^{-0.8} \left(\frac{V_c y_c}{\nu}\right)^{0.2} \tag{34}$$

Hartnett et al:[37]

$$\eta = 3.39 \left(\frac{V_g x}{V_c y_c}\right)^{-0.8} \left(\frac{V_c y_c}{\nu}\right)^{0.2} \tag{35}$$

In later work, the following expressions were deduced by Stollery:[46]

$$\eta = 3.09\left(\frac{V_{gx}}{V_{c}y_{c}}\right)^{-0.8}\left(\frac{V_{c}y_{c}}{\nu}\right)^{0.2} \tag{36}$$

Seban and Back:[45]

$$\eta = 11.2\left(\frac{V_{gx}}{V_{c}y_{c}}\right)^{-0.85}\left(\frac{V_{c}y_{c}}{\nu}\right)^{0.15} \tag{37}$$

Kutateladze and Leont'ev:[36]

$$\eta = 3.1\left[4.16 + \frac{V_{gx}}{V_{c}y_{g}}\left(\frac{V_{c}y_{c}}{\nu}\right)^{-0.25}\right]^{-0.8} \tag{38}$$

Librizzi and Cresci:[1]

$$\eta = 3.0\left[3.0 + \left(\frac{V_{gx}}{V_{c}y_{c}}\right)^{0.8}\left(\frac{V_{c}y_{c}}{\nu}\right)^{-0.2}\right]^{-1} \tag{39}$$

Stollery and El-Ehwany[44] made a simplified derivation which equated the film cooling effectiveness in terms of enthalpy. This expression, which obtained good correlation to experimental data, is:

$$\eta' = 3.09\left(\frac{V_{gx}}{V_{c}y_{c}}\right)^{-0.8}\left(\frac{V_{c}y_{c}}{\nu}\right)^{0.2} \tag{40}$$

where

$$\eta' = \frac{H_{ad} - H_{g}}{H_{c} - H_{g}} \tag{41}$$

Recently, Spaulding[43] presented a comparison of the theories of most of the authors mentioned above in predicting the adiabatic wall temperature in film cooling systems. To emphasize the similarities in the theories, he restricted his discussion to two-dimensional, uniform-property flows. As a result of comparing the theories and comparing experimental data from several different sources, an artificially contrived equation was proposed that would reasonably fit all the experimental data corresponding to velocity ratios of coolant to mainstream, V_c/V_g, for values ranging from nearly 0 up to about 14, and data taken from different shapes of geometrical arrangements at the slot. The results can be expressed, for uniform properties, as follows:

for $X < 7$: $\eta = 1$ (42)

for $X \geq 7$: $\eta = \frac{7}{X}$ (43)

where

$$X \equiv 0.91 \left(\frac{V_g x}{V_c y_c}\right)^{0.8} \left(\frac{V_c y_c}{\nu}\right)^{-0.2} + 1.41 \left\{\left|1 - \frac{V_g}{V_c}\right| \cdot \frac{x}{y_c}\right\}^{0.5} \quad (44)$$

Although this theory is not exact, Spaulding has shown that it can be used over a broad range of geometrical slot arrangements and V_c/V_g with fair correlation to experimental data. Figure 21 shows the correlation obtained with this theory.

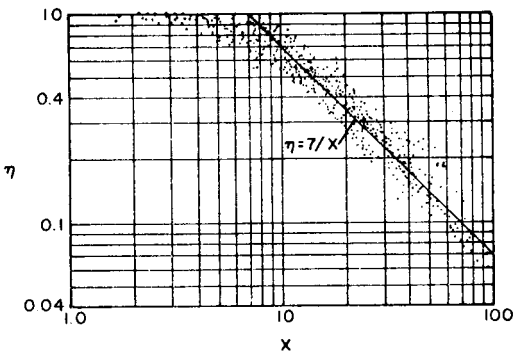

Figure 21. Agreement Between Equation (44) and the Data of Various References[43]

Perhaps the closest simulation and the most flexible theory was developed by Hatch and Papell.[42] Later investigators[5,47,48,49] have used this simulation to correlate their test results with reasonably good results. In contrast to most other theoretical models, the Hatch and Papell model begins by assuming that the coolant film exists as a discrete layer (no mixing). Two empirical modifications are then made to take care of the mixing phenomenon. This model provides a good basis for correlating experimental data taken reasonably close to the coolant slot $(0 < x/S < 150)$.[44]

The Hatch and Papell film cooling correlating equation, developed for relatively high gas stream temperatures, was used on a simplified theoretical heat-transfer model and qualified by empirically determined constants and parameters. Although this equation was developed by

using data covering a wide range of coolant gas properties and values of basic parameters, it was, however, limited to tangential injection of the coolant parallel to an adiabatic wall. Subsequently, Papell[50] presented further semiempirical corrections to be applied to the equation to correct data obtained with coolant injection through angled slots and normal holes. Data were obtained for coolant injection through slots at angles up to and including 90 degrees relative to the adiabatic wall and also through rows of normal holes. These data were restricted to subsonic flow with no pressure gradient in the flow direction. The Hatch-Papell equation for gaseous film cooling of angled slots is as follows:

$$\ln \eta = \ln\left(\frac{T_{ad} - T_{ad'}}{T_{ad} - T_c}\right) = -\left(\frac{h_g L x}{(\dot{w}C_p)_c} - K\right)\left(\frac{SV_g}{a_c}\right)^{1/8} f\left(\frac{V_g}{V_c}\right) + \ln \cos 0.8\,\beta_{eff} \tag{45}$$

where

$$f\left(\frac{V_g}{V_c}\right) = 1 + 0.4 \tan^{-1}\left(\frac{V_g}{V_c} - 1\right) \qquad \text{for } \frac{V_g}{V_c} \geq 1.0 \tag{46}$$

$$= \left(\frac{V_c}{V_g}\right) 1.5\left(\frac{V_c}{V_g} - 1\right) \qquad \text{for } \frac{V_g}{V_c} \leq 1.0 \tag{47}$$

where

$$\beta_{eff} = \tan^{-1}\left(\frac{\text{Sin } \beta}{\text{Cos } \beta + \frac{(\rho V)_g}{(\rho V)_c}}\right) \tag{48}$$

and where all angles are in radians. With only convective heat transfer, K=0.04. The equation assumes that there is no heat addition to the cooled wall, that is, $T_{ad'}$ is the adiabatic value of wall temperature reached with film cooling. The heat transfer coefficient, h_g, is measured at the slot location without cooling, the velocities are computed at the slot location, and all the coolant properties are computed at the temperature and pressure of the coolant as it emerges from the slot.

The correlating equation developed for slot injection of the coolant [Equation (45)] contained a discrete value of slot height as a basic parameter and, therefore, could not be applied to the hole configuration data. A modification was made by defining an effective slot height S' as the total coolant flow area divided by the width of the first row of holes, $S' = A_c/y$. Further, for values of velocity ratio greater than unity, it was found that a corrective term for the modified slot correlating equation equal to $-0.08\left(V_g/V_c\right)$ generalized the data. The resulting

correlating equation for normal hole injection of the coolant is:

$$\ln \eta = -\left(\frac{h_g L x}{(\dot{w} C_p)_c} - K\right)\left(\frac{S' V_g}{a_c}\right)^{1/8} f\left(\frac{V_g}{V_c}\right) + \ln \cos 0.8\beta_{eff} - 0.08\left(\frac{V_g}{V_c}\right)_{V_g > V_c} \quad (49)$$

Sellers[51] has shown that Equation (45) can be used for multiple-slot correlation as well as single-slot. The adiabatic wall temperature with gaseous film cooling, $T_{ad'}$, is determined from Equation (45). Now, assume that a new slot is introduced downstream. Again, the adiabatic wall temperature is determined from Equation (45), but note that the adiabatic wall temperature without film cooling, T_{ad}, is a function of the distance downstream of the slot, x, and is actually the $T_{ad'}$ curve from the original slot. The procedure is repeated if additional slots are added, noting that T_{ad} is different for each slot and each time is equal to the $T_{ad'}$ results from the preceding slot. Sellers used the foregoing concept to show rather good agreement between the experimental and calculated wall temperatures using 2, 3, 4, and 5 slots of various dimensions. In correlating his data, Sellers used K = 0 rather than K = 0.04 as shown in Equation (45) since, he indicates, there is some evidence from rocket engine film-cooling experiments that a value of K = 0.04 may be too large.

(2) Experimental Investigations. Most experimental data obtained for gaseous film cooling have been for cylindrical combustion chamber sections. The literature shows few experimental studies on gaseous film cooling of nozzles at high free stream temperatures.[5, 51, 52] Some experimental data have been obtained at relatively low nozzle temperatures.[32, 48, 49, 53]

The Marquardt Corporation[5] made film cooling calculations using the Hatch-Papell equation for several coolants and nozzle configurations to provide a comparison of conventional film cooling analysis with their experimental results. The analytical and experimental studies included a two-row hole pattern, a tangential slot, and multislots.

When multislot cooling was used, the analysis procedure was modified to account for the effect of upstream film cooling by using an adiabatic wall temperature at any location which was the same as the wall (i.e., recovery) temperature which would have been predicted at that location from the upstream cooling alone. This is the modification which was discussed by Sellers[51] as mentioned previously. The multislot nozzles tested were designed as shown in Figure 22. The hydrogen cooling requirements for various values of maximum wall temperature are shown in Figure 23. Although four test runs were made on this

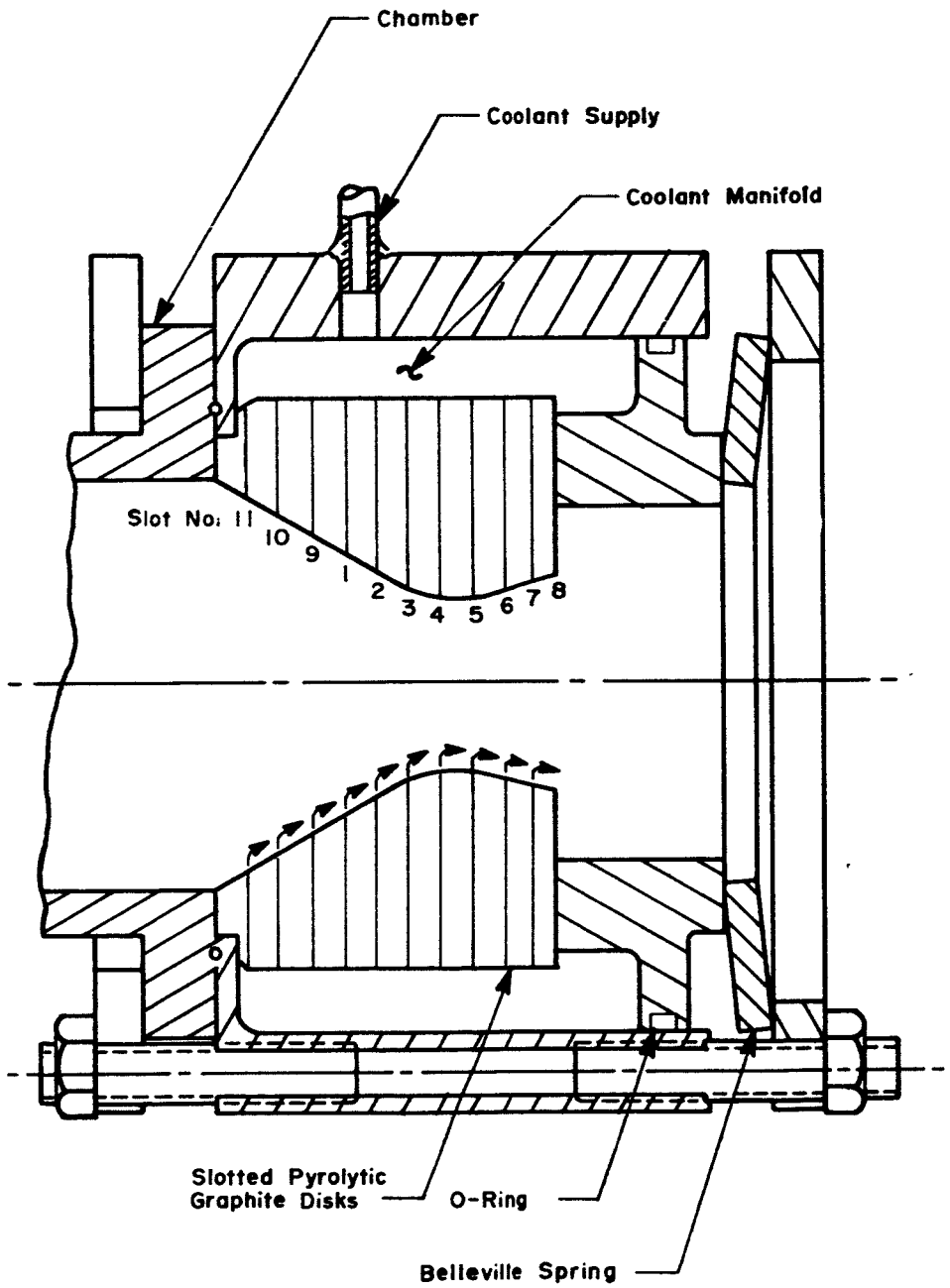

Figure 22. Multislot, Film Cooled Pyrolytic Graphite Nozzle[5]

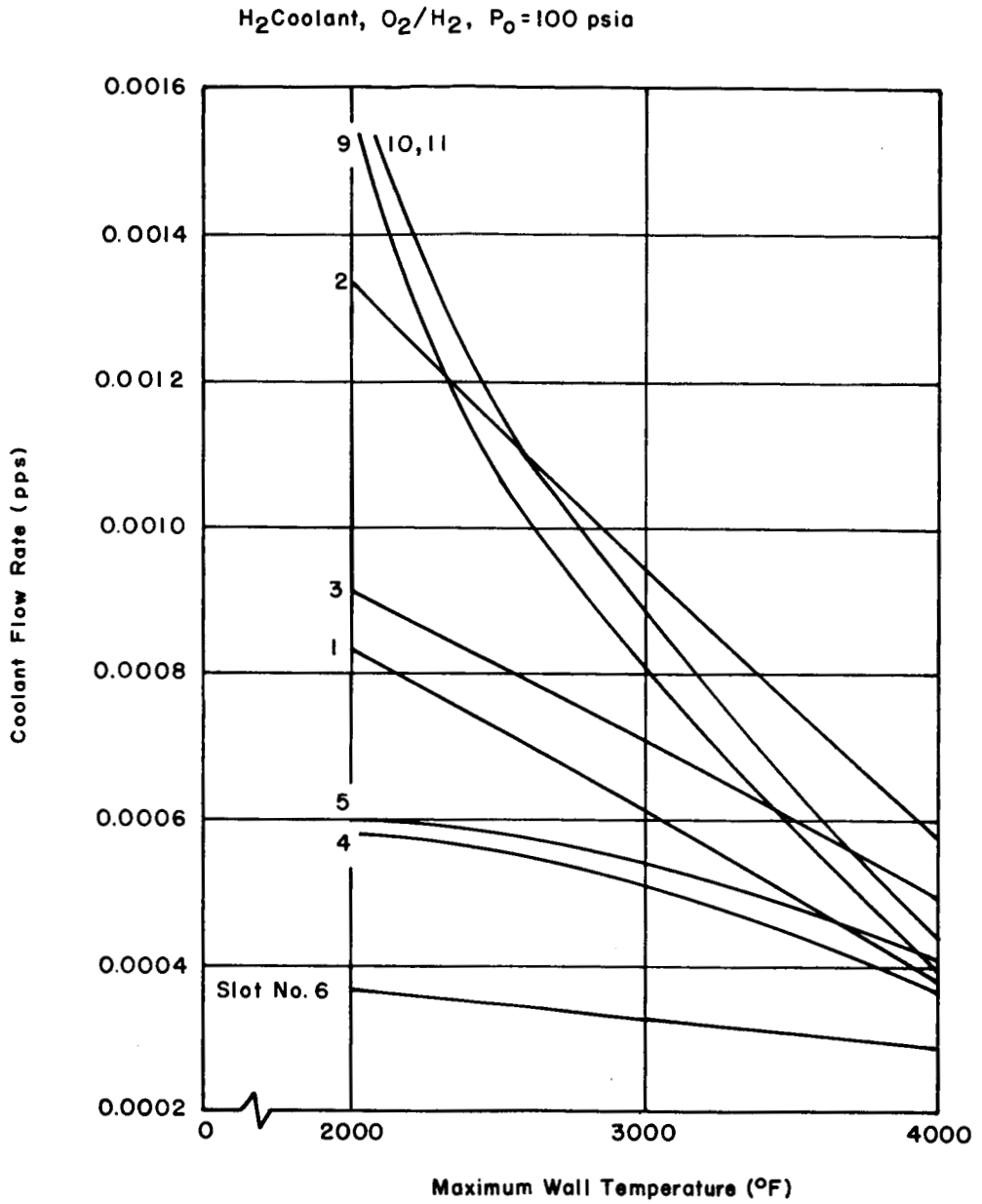

Figure 23. Gaseous Film Cooling for Standard Nozzle with Multislot Cooling[5]

nozzle configuration, using hydrogen, methane, and carbon monoxide as coolants, a comparison of theoretical and experimental results was not reported upon. (The end result of the test was to determine throat erosion--methane and hydrogen induced none and carbon monoxide induced a slight amount.) However, it was concluded that multislot cooling is a most promising means of cooling when high energy propellants are used.

The variation of analytical and experimental nozzle temperature with coolant flow rate for single slot injection is shown in Figure 24 for hydrogen cooling and in Figure 25 for helium cooling. The limited data indicate that helium is about as good as hydrogen as a film coolant on an equal weight flow basis, rather than being inferior by a 3:1 weight flow ratio as was predicted analytically.

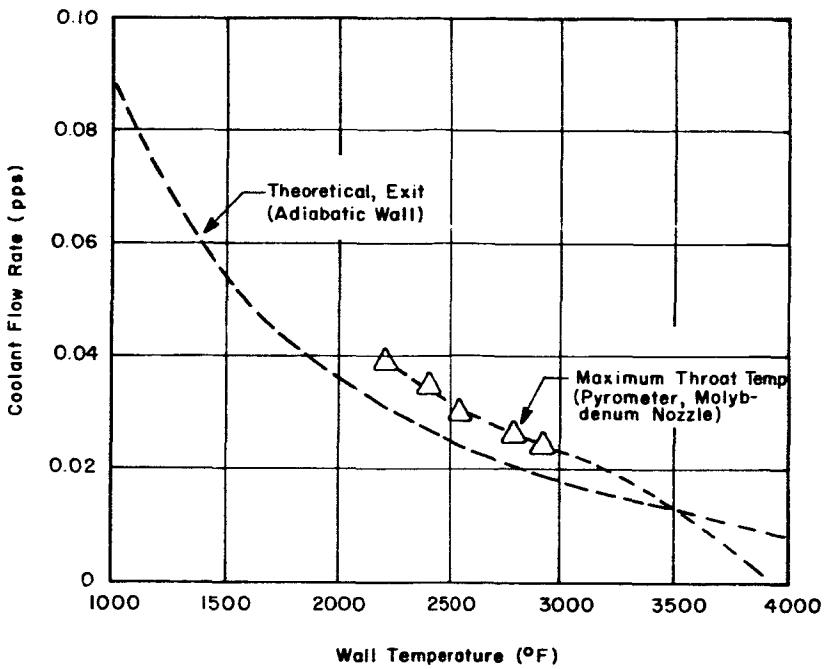

Figure 24. Variation of Analytical and Experimental Nozzle Temperatures with Flow Rate-Radiation/Hydrogen Film Cooling[5]

The effect on thrust of film cooling with hydrogen, helium, and methane is shown in Figure 26. The data show that methane cooling may incur a large loss in performance, whereas small amounts of helium can be used with no loss of performance. Indeed, some of the data for helium show an increase above the performance without cooling. The one available point for hydrogen cooling shows a surprising result in that no loss in specific impulse was indicated.

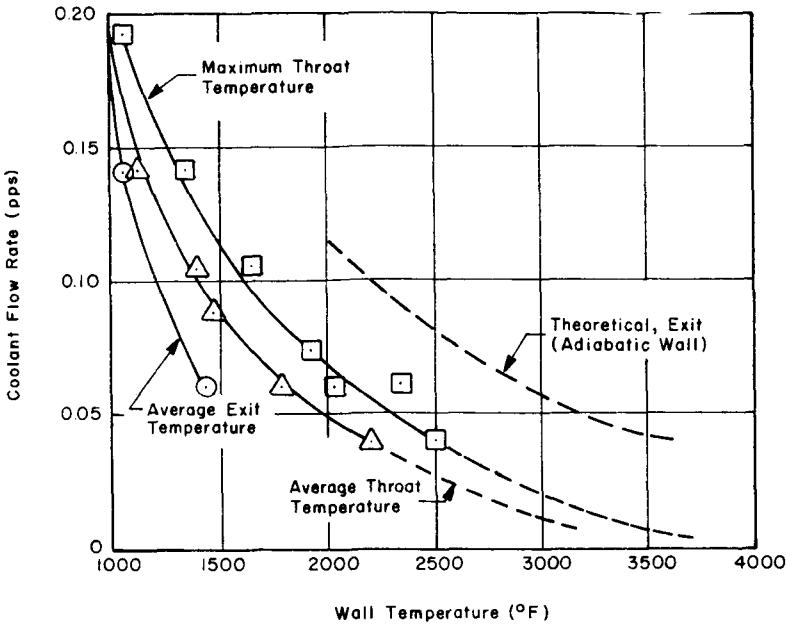

Figure 25. Variation of Analytical and Experimental Nozzle Temperatures with Flow Rate - Radiation/Helium Film Cooling[5]

b. Liquid Film Cooling

The mechanism of liquid film cooling has been well documented and a summarization of the results of many of the investigations is available.[54] As with gaseous film cooling, most of the experimentalists have studied cooling of cylindrical sections and little work has been done on nozzles. Even in cylindrical flow, the various investigators do not agree, primarily on the effective heat transfer coefficient.[54] The investigators of gaseous film cooling have introduced empirical parameters involving dimensions of injection slots, velocity of injected coolant, and other parameters which cannot be easily applied to the vapor phase of liquid film cooling. Therefore, most of the theoretical work on gaseous film cooling cannot be applied directly to the theory of liquid film cooling. As mentioned before, the effect on film stability of adverse pressure gradients has not been satisfactorily determined.

(1) Theoretical and Experimental Study by Emmons[31].

One notable experimental investigation and analytical study on liquid film cooling was carried out by Emmons who obtained information regarding the effect of the gas stream temperature, pressure, Reynolds number, and physical properties of the film coolant upon the convective heat transfer coefficient between the hot gas stream and the surface of the liquid film, and obtained information concerning the insulation effect

provided by the film coolant vapor for the area downstream from the liquid film. These studies were made on a horizontal 3-inch-inside diameter film cooled combustion chamber which was placed between two convectively cooled chambers. Hydrogen-air combustion gas was used at pressures from 250 to 750 psia and temperatures from 2600° to 4100°R with a gas stream Reynolds number of 0.55 (10^5) to 1.83 (10^5). Water, anhydrous ammonia, ethyl alcohol, and Freon 113 liquid film coolants were introduced tangentially. The film cooled combustion chamber was instrumented to determine the wall temperature.

Figure 27 is typical of the data obtained, which shows how the wall temperature varies with coolant flow rate. Figure 28 shows the linear dependence of the cooled length (which is defined as the chamber length, which is below the boiling point of the coolant) on coolant flow. Figure 29 presents the experimentally determined values of the film-cooled length as a function of the film coolant flow rate. The curve was obtained by the method of least squares. The results indicate that the combustion pressure, within the range 250 to 750 psia, has an insignificant influence upon the flow rate of the film coolant required for cooling a given film-cooled length. Figure 30 presents the experimentally determined film-cooled length as a function of the required coolant flow rate when the combustion pressure and Reynolds number are held constant. Figure 31 shows the film-cooled length as function of film coolant flow rate when the combustion temperature and pressure were maintained constant.

(a) Liquid Phase - The analytical analysis made by Emmons for the liquid cooling is derived for the case of turbulent incompressible flow of the hot gas stream. The flow model employed consisted of a turbulent stream of hot gas flowing over a stable liquid film having a uniform temperature equal to the boiling point of the liquid. The coolant is assumed to evaporate from the liquid film surface at a uniform rate and diffuse into the hot gas stream within a sublayer region adjacent to the liquid surface with a velocity equal to the film coolant flow rate per unit surface area Q divided by the specific weight of the coolant γ_c. The velocity profile within the sublayer is based upon a diffusivity variation relationship which takes into account the vapor injection velocity at the wall.

The expression relating the heat transfer coefficient h_f between the liquid film surface and the hot gas stream and the film coolant derived by Emmons is as follows:

$$h_f = \frac{k_v \tau_{wo}}{\mu V_g} \left(1 - \frac{13.89Q}{b\gamma_c \sqrt{\frac{\tau_{wo}}{\rho}}} \right) \qquad (50)$$

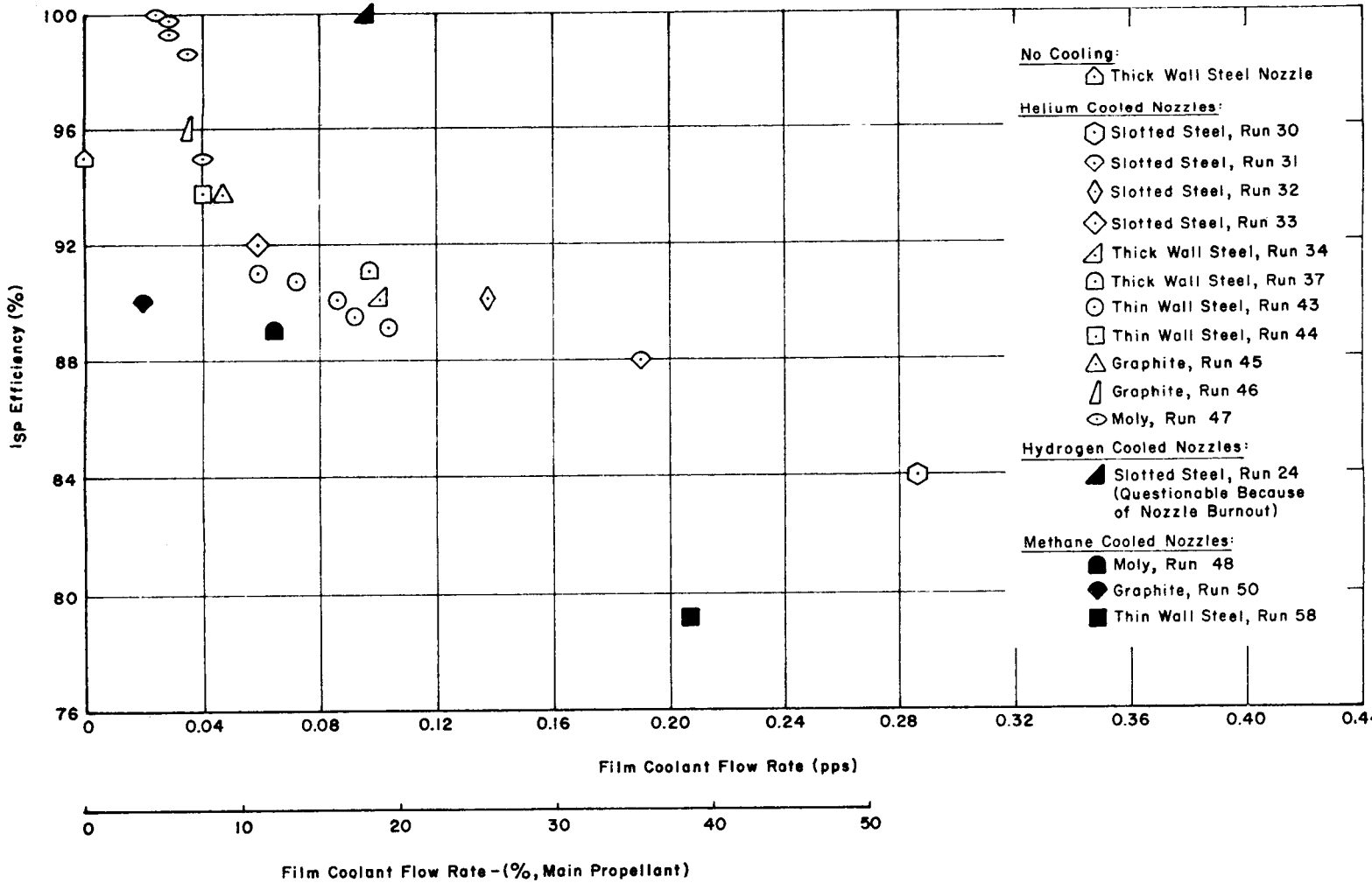

Figure 26. Variation of Specific Impulse Efficiency with Film Coolant Flow Rate for Helium, Hydrogen, and Methane[5]

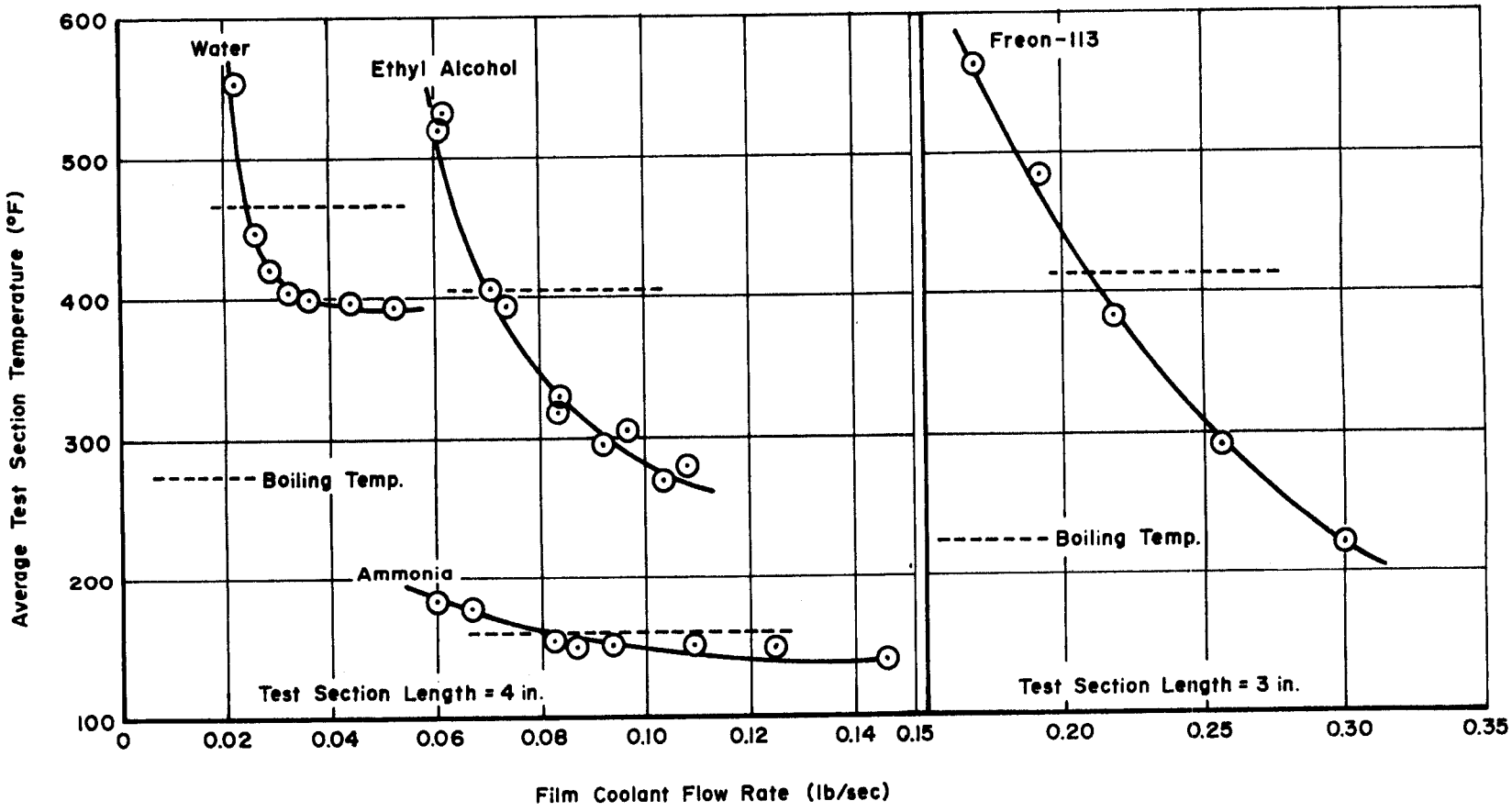

Figure 27. Variation of Average Test Section Temperature with Film Coolant Flow Rate for Different Film Coolants [31]

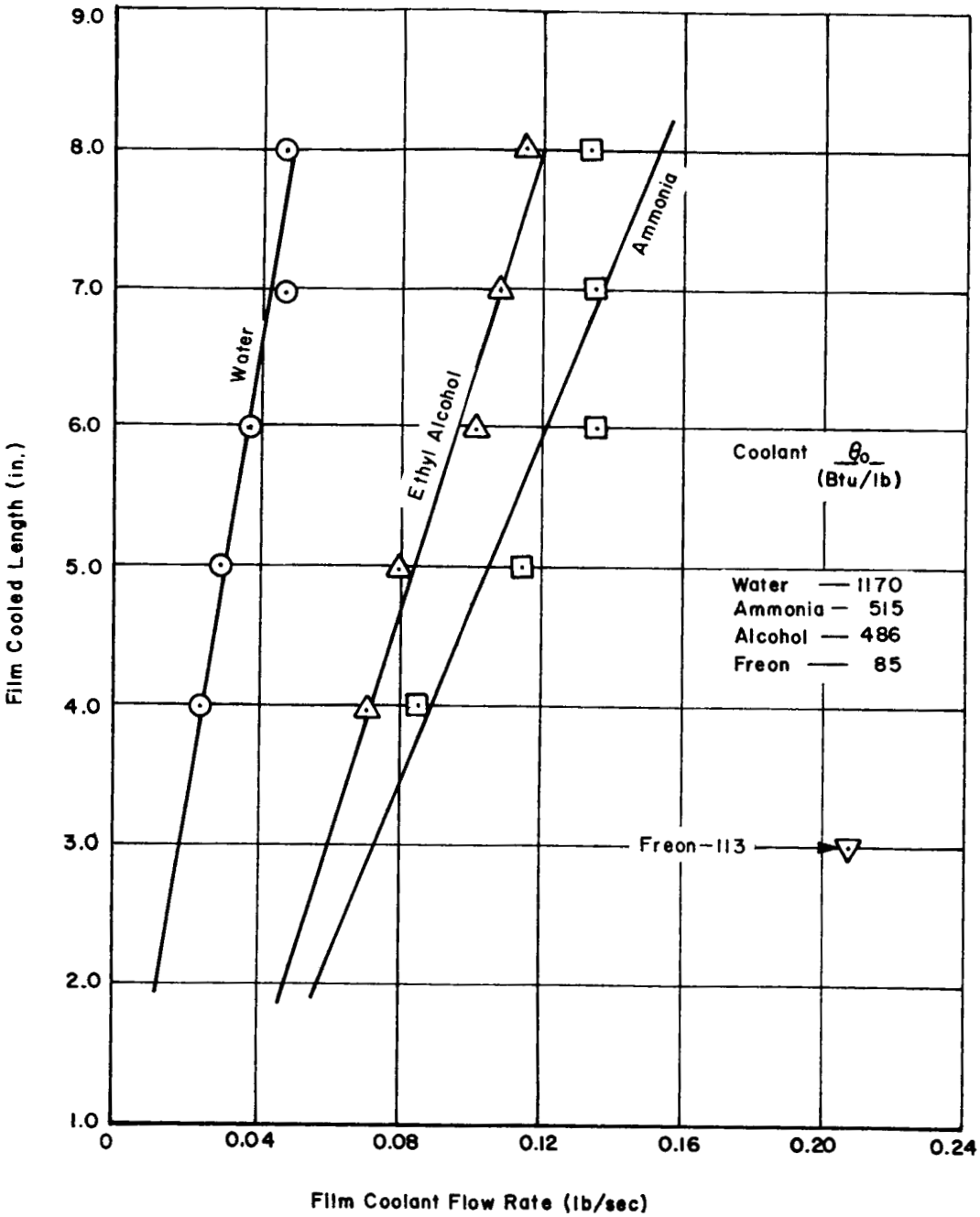

Figure 28. Variation of Film-Cooled Length with Film Coolant Flow Rate for Different Film Coolants [31]

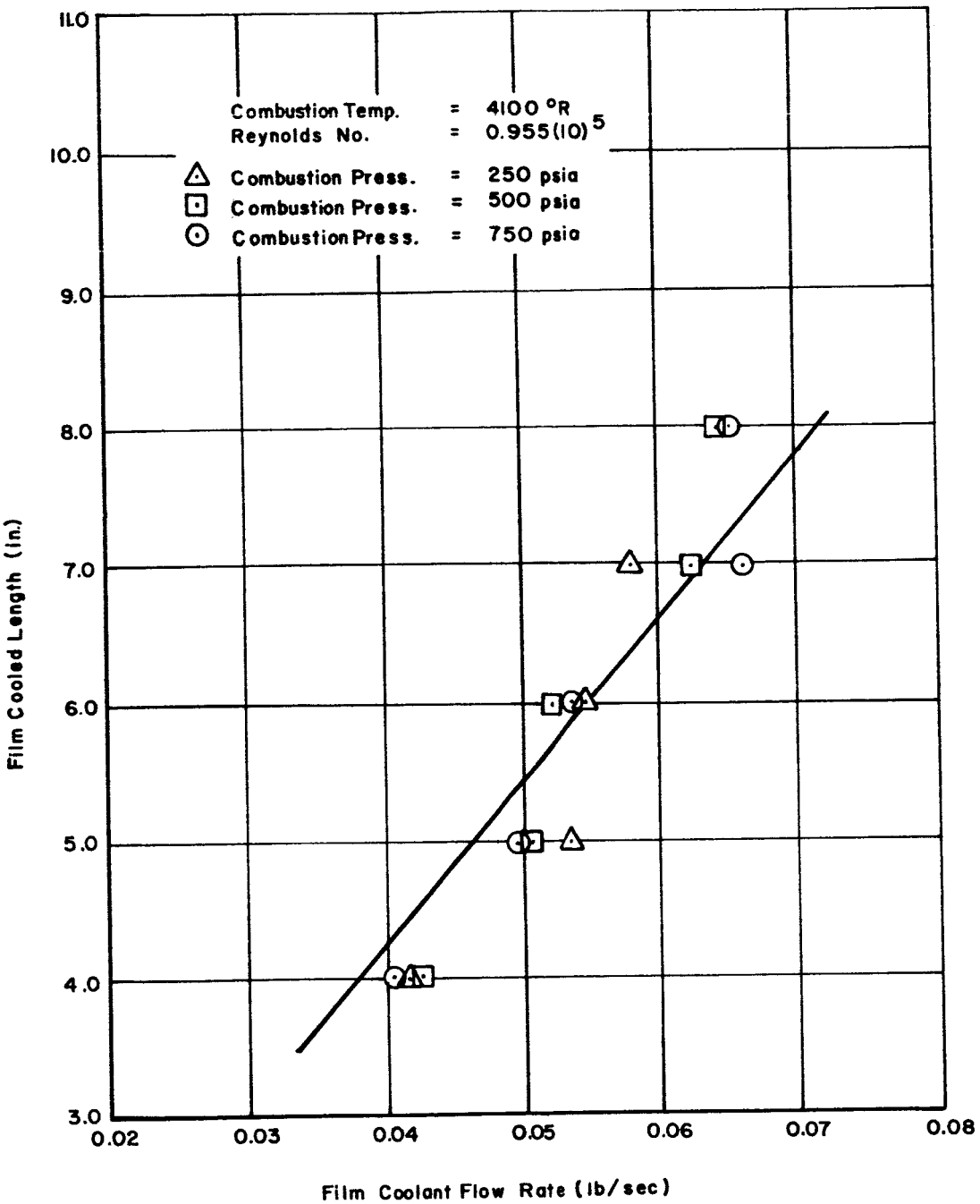

Figure 29. Variation of Film-Cooled Length with Film Coolant Flow Rate for Different Combustion Pressures - H_2O Film Coolant [31]

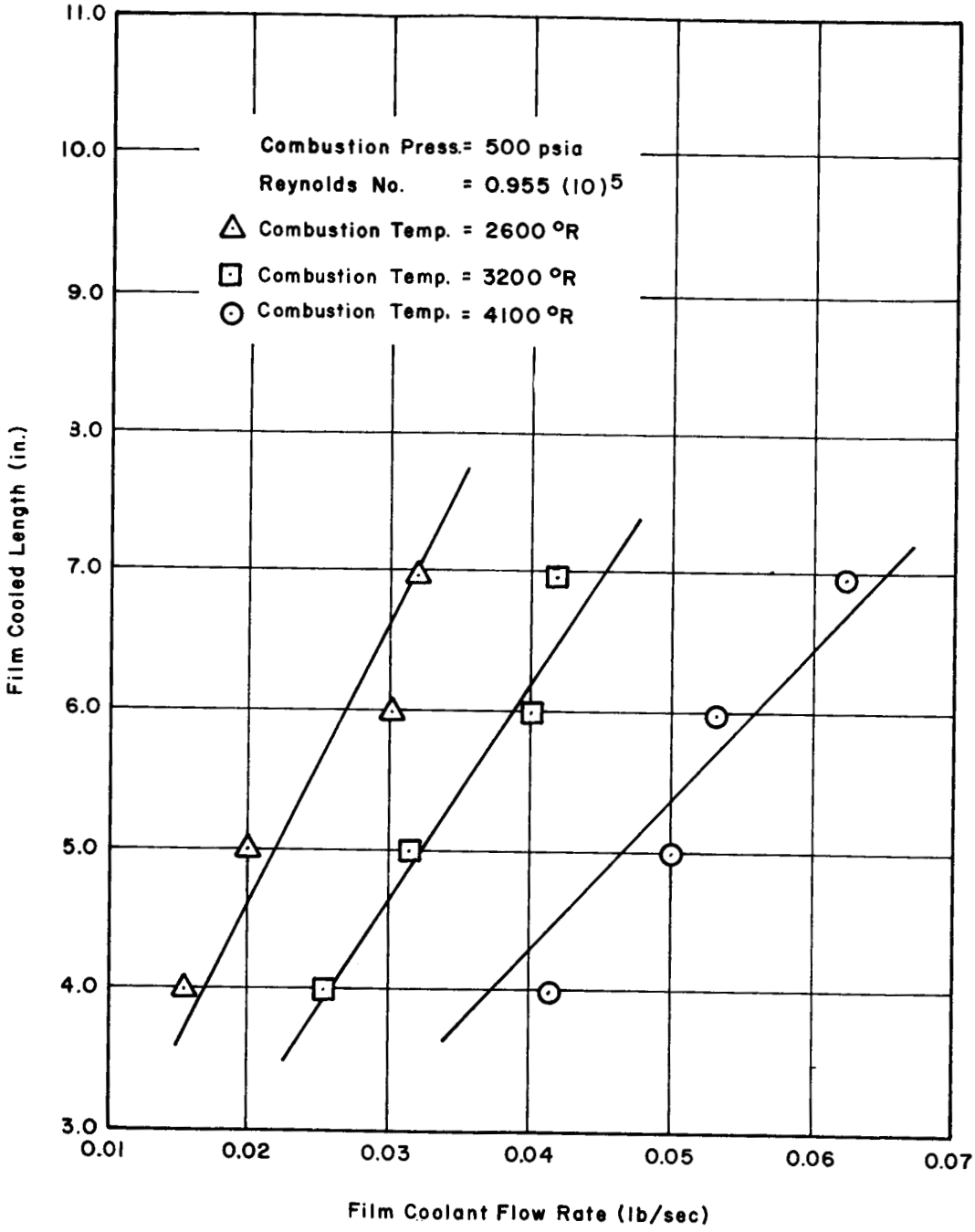

Figure 30. Variation of Film-Cooled Length with Film Coolant Flow Rate for Different Combustion Temperatures - H_2O Film Coolant [31]

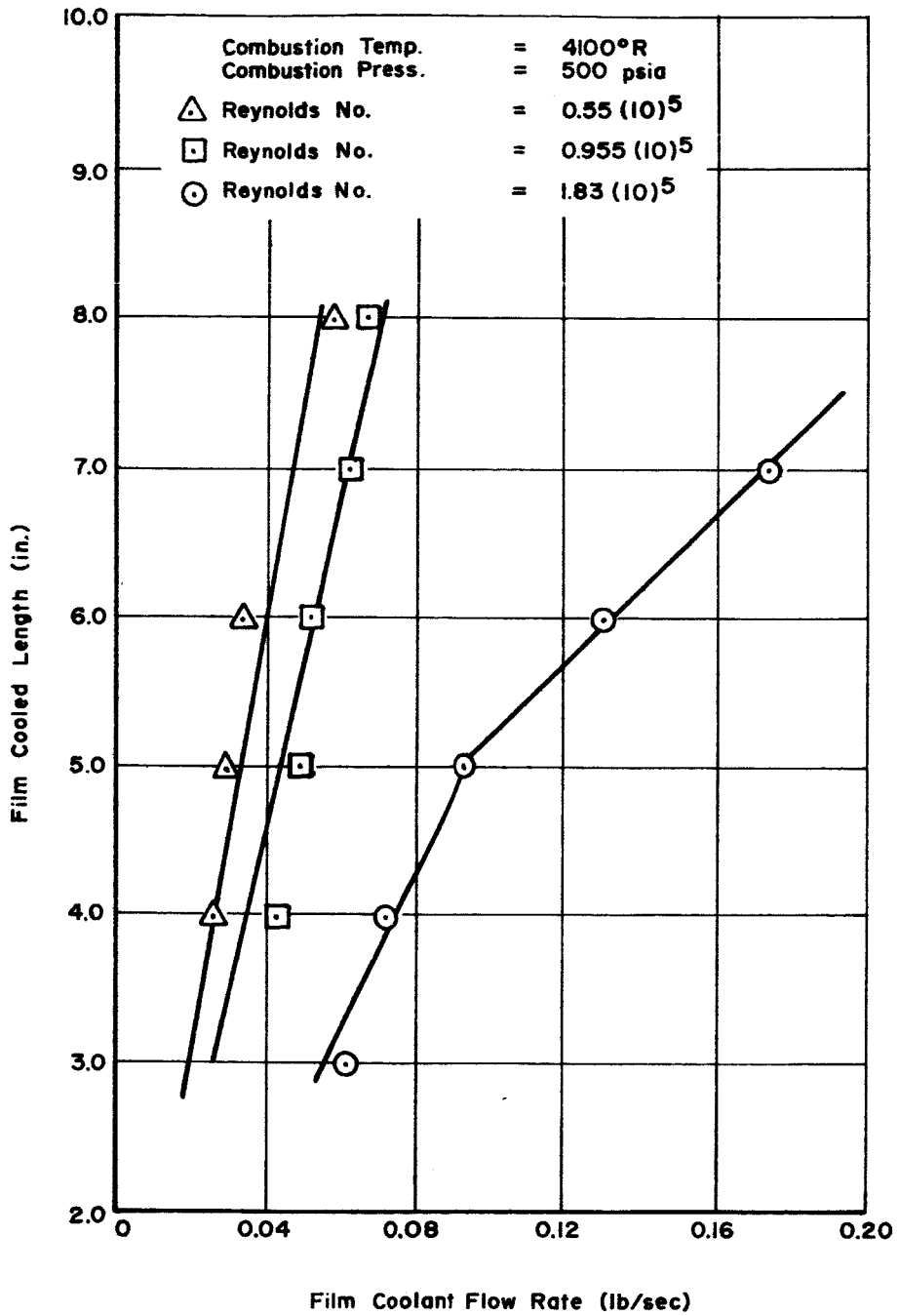

Figure 31. Variation of Film-Cooled Length with Film Coolant Flow Rate for Different Main Stream Reynolds Numbers - H_2O Film Coolant [31]

in which h_f is defined in terms of the gas stream temperature T_g, the liquid film surface temperature T_v, and the rate of heat transfer q by the expression:

$$q = h_f \left(T_g - T_v\right) \tag{51}$$

The relationship between θ_o and h_f is given by:

$$h_f = \frac{Q\theta_o}{T_g - T_v} \tag{52}$$

Emmons used Equation (52) to calculate the heat transfer coefficient for the liquid film by employing various values of film coolant flow rate Q.

An expression was derived for the ratio of film coolant flow rate Q to the mass velocity of the gas stream G in terms of the pertinent physical properties of the gas and coolant as follows:

$$\frac{Q}{G} = V_m k_v \left(T_g - T_v\right)\left(\frac{2\gamma_g\theta_o\nu}{F_o} - \frac{13.89\ \gamma_g V_m k_v \left(T_g - T_v\right)}{b\,\gamma_c\sqrt{\frac{F_o}{2}}}\right)^{-1} \tag{53}$$

where the average calculated value of the empirical parameter b is 0.110.

Since the Nusselt number is defined by:

$$Nu = \frac{h_f D}{k_g} \tag{54}$$

an expression was derived for the Nusselt number applicable for liquid film cooling by substituting Equations (52), (53), and (54), rearranging and simplifying.

$$Nu = \frac{F_o Re}{2}\left(\frac{V_g k_g \nu}{V_m k_v \nu_s} - \frac{89.3\sqrt{F_o}\,k_g\left(T_g - T_v\right)}{\gamma_c\theta_o\nu_s}\right)^{-1} \tag{55}$$

(b) Vapor Phase - Data obtained from the convectively cooled combustion chamber downstream of the film cooled unit indicated that a cooling effect occurred even though no liquid was present. Apparently, the cold vapor blanketed the wall from the hot gas stream for some distance.

For the vapor phase, Emmons employed a flow model similar to that employed by Hatch and Papell, with the exception that the restriction of an adiabatic wall was removed. The final result of the analysis was the development of the following equation relating the heat flux and wall temperature distribution to the film coolant flow rate:

$$\ln \eta = \ln \frac{T_g - T_w - \frac{2q_w}{h_v}}{T_g + T_w - 2T_v} = - \frac{2\pi D h_g x}{\dot{w}_{fc} C_{pc}} \tag{56}$$

To correlate with experimental data, Equation (56) was modified to account for the flow conditions of the hot gas stream. An empirical function, in terms of the flow rate ratio, was determined that best correlated the experimental data for vapor film cooling. The final equation for correlating the data is:

$$\ln \eta = - \frac{2\pi D h_v x}{\dot{w}_{fc} C_{pc}} f\left(\frac{\dot{w}_g}{\dot{w}_{fc}}\right) \tag{57}$$

where

$$f\left(\frac{\dot{w}_g}{\dot{w}_{fc}}\right) = 1 + 0.25 \tan^{-1} \left(15 - \frac{\dot{w}_g}{\dot{w}_{fc}}\right) \tag{58}$$

and where the angle in the empirical function (Equation 58) is expressed in radians.

Figure 32 presents the results of plotting the semitheoretical Equation (57) with experimental data. Using the empirical function (Equation 58) in conjunction with Equation 57 corrects the experimental data with reasonable accuracy for ammonia. Since the data for water (Figure 33) exhibited a greater degree of scatter, Emmons concluded that the empirical function $f\left(\dot{w}_g / \dot{w}_{fc}\right)$ does not correlate the data with the desired degree of accuracy at larger values of the flow rate parameter. He hypothesized that much of the data scatter was caused by turbulent mixing between the gas stream and the film coolant. (Turbulent mixing was neglected in the analysis.)

(2) Theory Used by Marquardt Corporation[54]. For liquid film cooling in the nozzle section, Marquardt Corporation used the Stanton number for smooth flow and applied the following equation to be integrated over the section of interest:

$$\frac{d\dot{w}_c}{\dot{w}_g} = \frac{2\, St_i\, C_{p_g} \left(T_g - T_w\right)}{\left(\frac{A}{A^*}\right)^{1/2} \Delta H_c} \left(\frac{\pi C_F P_i}{T}\right)^{1/2} dx \tag{59}$$

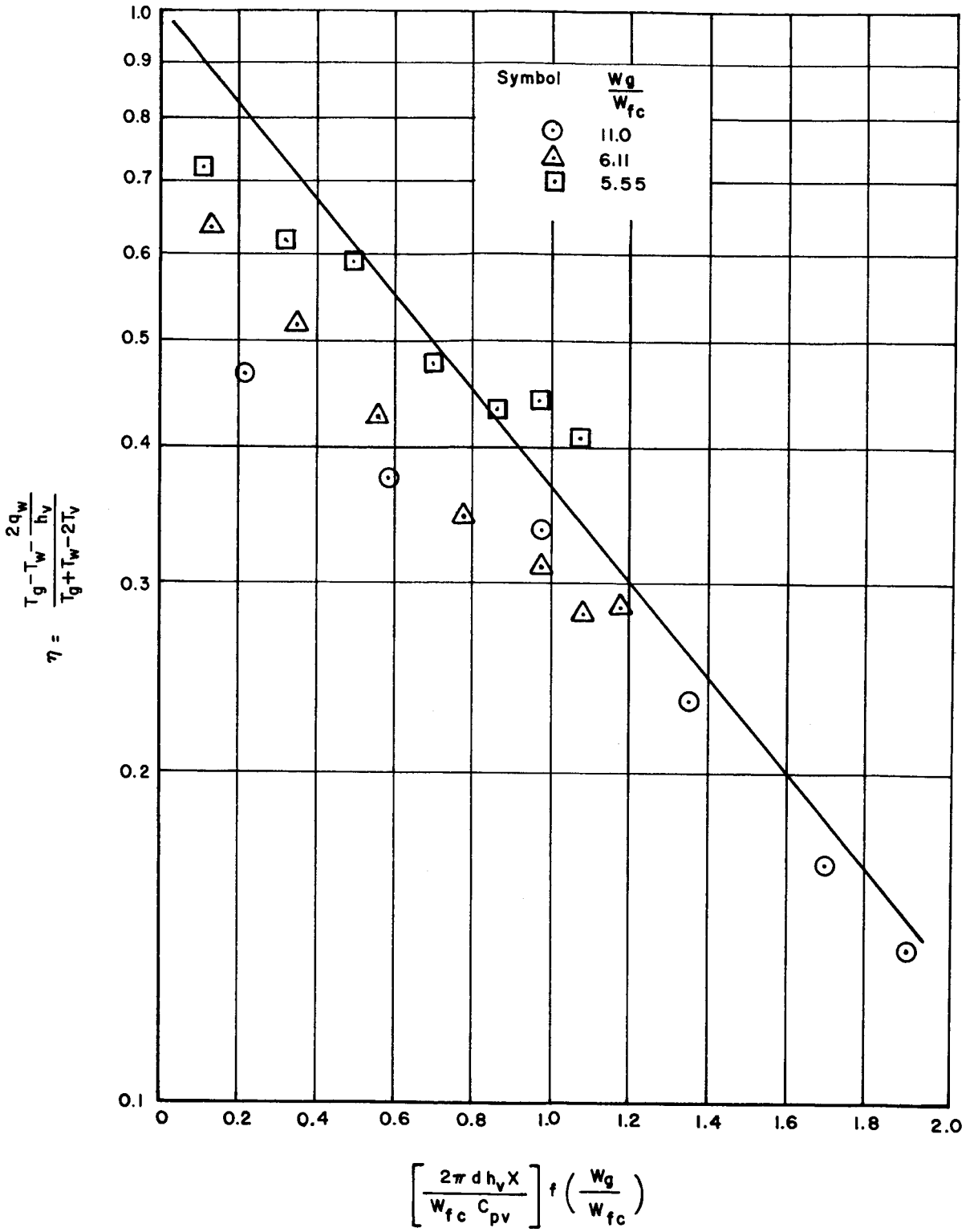

Figure 32. Temperature Ratio Parameter as a Function of the Length Parameter for Ammonia Film Coolant - Gas Stream Reynolds Number = 0.55 (10^5)

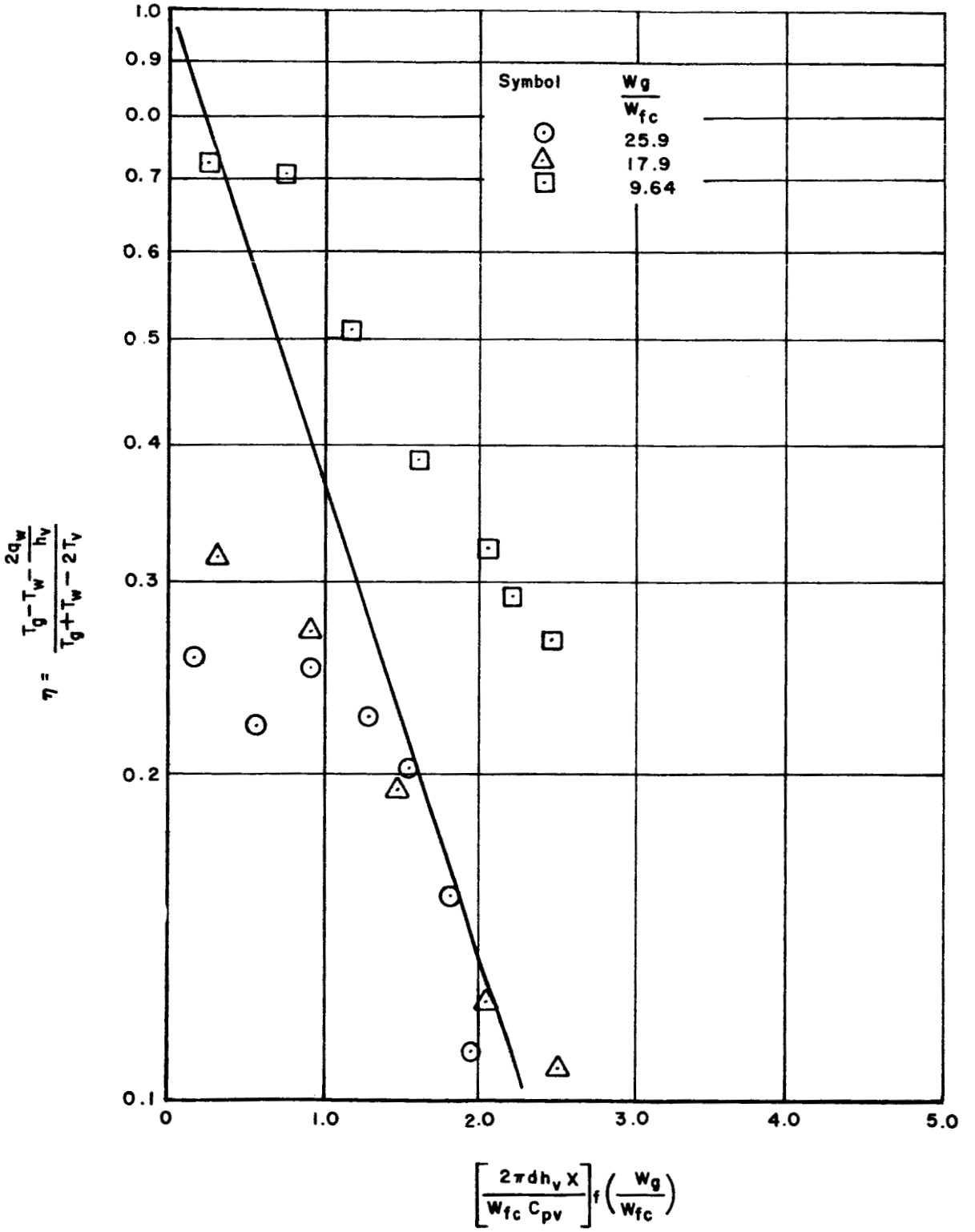

Figure 33. Temperature Ratio Parameter as a Function of the Length Parameter for Water Film Coolant - Gas Stream Reynolds Number = 0.55 (10^5)

Equation (59) represents a conservative approach since the cooling ability of the vapor downstream from the liquid was neglected. The cooling effect of the vapor might be quite large when considering a coolant which has a low heat of vaporization and a high specific heat. However, at the time Marquardt Corporation made their analysis, and subsequent to that time, the literature did not show a good correlating equation to predict the effect of vapor cooling downstream from the liquid.

(3) Experimental Study by Marquardt Corporation[55]. Marquardt Corporation made a study on the behavior of a liquid film in a typical nozzle throat. The study included the spreading of the film introduced at discrete points, the stability of the film, and the cooling effect of the film. The three-dimensional test nozzle was the convergent-divergent type having a 12.8-degree inlet half angle, a 3.4-degree exit half angle, and a 1.3-inch throat diameter. The nozzle was comprised of three copper segments, one comprising the inlet up to the throat and two making up the exit. Between the segments were brass coolant injection rings, through which water coolant was injected independently by each segment. Water coolant was injected at the nozzle inlet plane, at the throat, and between the throat and exit plane. The coolant exit velocity component was tangent to the nozzle wall and perpendicular to the gas stream.

Table V lists the test results obtained with the three-dimensional nozzle, along with theoretically required coolant flow rates calculated on the basis of a Stanton number of 0.003, calculated coolant manifold gas stream pressure differentials, and the coolant head pressures across the injection rings.

The test on the three-dimensional nozzle verified the results obtained from prior tests on two-dimensional nozzles. The following conclusions were drawn:

1) The location of liquid injection is an important factor to achieve best film cooling performance. In general, the coolant should be injected at locations where it is least subject to the generation of instabilities by the gas stream.

2) Injecting the liquid in a straight converging section and at the throat provides the best liquid film cooling performance.

3) Inefficiency in film cooling is caused by film instability resulting in liquid loss to the gas stream prior to evaporation.

Table V. Test Results for Three-Dimensional Film Cooled Nozzle[55]

	Inlet Segment		Center Segment		Last Segment	
	Upper	Lower	Upper	Lower	Upper	Lower
Wall temperatures, °R	840	745	790	755	765	800
Coolant saturation temperature, °R, at thermocouple locations	850		797		770	
Actual coolant flow rate, lb/sec	0.10		0.083		0.033	
Theoretically required coolant flow rate, Stanton number = 0.003, lb/sec	0.0427		0.0315		0.0222	
Calculated coolant manifold - gas stream pressure differential - using value of coolant viscosity at its normal boiling point - replacing coolant passage with round passage of equal perimeter, psi	1.31		1.33		0.832	
Coolant head between highest and lowest points of injection ring outer diameter, psi	0.0942		0.0830		0.0874	

NOTE: Test Conditions: $\dot{w}_g$ = 4.6 lb/sec, T_g = 3600°R, P_g = 405 psia

4) Film instability is caused by interaction of the gas stream on the liquid film. Thick film and film flow maldistribution aid instability.

5) Direct correlation of the instability behavior in the tests was not possible due to the complexity of thin film instability.

6) Satisfactory film distribution at injection can be achieved by designing the injector to have a pressure differential of at least ten times greater than other forces affecting coolant distribution, such as gravity head in a horizontally mounted nozzle.

(4) Computer Program Development. Aerojet-General Corporation[11] is developing a computer program (8083) to evaluate the effectiveness of film cooling and regenerative cooling at very high thrust chamber pressures for a liquid rocket thrust chamber cooled by a combination of film and regenerative cooling. This program is similar to an existing program, but incorporates several improvements which give results more closely approximating actual test data. The method used to calculate the temperature of the film in film cooling is basically that described by Hatch and Papell. The method of calculating the film cooling effectiveness and the manner in which it is used has been modified to conform to hot-firing data. Incorporated into the computer program are the physical properties of N_2O_4 and AeroZINE 50 which will allow the option of film cooling or regenerative cooling with either fluid.

3. List of Symbols for Film Cooling

A = Gas flow area.

b = Empirical parameter.

C_F = Rocket nozzle thrust coefficient.

C_p = Specific heat at constant pressure.

d = Differential of a function.

D = Inside diameter of the rocket motor chamber.

D_h = Hydraulic diameter.

f = Function.

F = Fanning friction coefficient.

G = Gas mass velocity.

h = Convective heat-transfer coefficient $\left[0.0265 \frac{k_f}{D_h} (Re)_f^{0.8} (Pr)_f^{0.3}\right.$ for gaseous film cooling$\left.\right]$.

H = Enthalpy.

ΔH_v = Heat of vaporization of the liquid film coolant.

k = Coefficient of thermal conductivity.

K = Constant; 0.04 with only convective heat transfer.

L = Width of adiabatic wall.

Nu = Nusselt number.

P = Pressure.

Pr = Prandtl number.

Q = Film coolant flow rate per unit surface area.

q = Heat transfer rate per unit area.

Re = Reynolds number.

S = Coolant slot height.

S' = Effective coolant slot height, A_c/y.

St = Stanton number.

t = Static temperature.

T = Stagnation temperature.

T_{ad} = Adiabatic wall temperature without film cooling.

$T_{ad'}$ = Adiabatic wall temperature with film cooling.

T_c = Temperature of coolant at exit slot.

V = Velocity.

$\dot{w}$ = Flow rate.

x = Distance along wall.

X = Dimensionless distance.

y = Width of first row of holes.

y_c = Width of slot in direction normal to wall.

α = Thermal diffusivity, $k/\rho C_p$.

β = Coolant injection angle relative to adiabatic wall.

β_{eff} = Effective coolant injection angle.

γ = Specific weight.

η = Cooling effectiveness.

$\theta_o = \Delta H_v + C_{pl}\left(T_v - T_o\right)$.

μ = Dynamic viscosity.

ν = Kinematic viscosity.

ν_s = Kinematic viscosity of gas evaluated at T_v.

ρ = Mass density.

τ = Shear stress.

Subscripts

ad = Adiabatic wall.

c = Coolant slot exit for gaseous film cooling and coolant for liquid film cooling.

f = Properties evaluated at $\frac{t_g + t_c}{2}$ for gaseous film cooling and liquid film for liquid film cooling.

g = Main body of gas.

l = Liquid.

m = Average conditions in the gas stream.

o = Dry wall.

w = Wall.

v = Vapor.

ch = Combustion chamber.

i = Initial or base condition.

Section IV. CONCLUSIONS

Although transpiration cooling in theory provides the greatest cooling effectiveness as compared to other cooling methods, this method has not been applied to the cooling of rocket engine nozzles. The problem of fabrication of porous shapes with uniform porosity as well as the necessary structural properties has not been completely solved.

Most analytical and experimental studies on transpiration cooling have been conducted by making several simplifying assumptions. These assumptions include flat plates rather than curved shapes, gaseous coolants, laminar flow, and temperature environments considerably lower than those encountered in high temperature liquid rocket nozzles. Before this form of cooling can be successfully applied, it is necessary to conduct extensive research under conditions that approximate closely those encountered in actual service.

Self-cooling has received considerable attention as a method of cooling solid propellant rocket nozzles and several tests proving its feasibility have been conducted. It appears that this form of cooling has not been considered at all for liquid rocket nozzles; however, based on the literature reviewed, there is no apparent reason why it cannot be used.

In gaseous film cooling, there is adequate analytical work, correlated with experimental data, to design a rocket nozzle cooling system and to predict the effectiveness of the coolant. Multislot cooling is very promising when high energy propellants are used. Gases with low molecular weight are more attractive as coolants because with their use there is less loss in specific impulse.

Although liquid film cooling has been combined successfully with other cooling techniques, there are presently no adequate analytical solutions verified by experimental data to predict the effectiveness of the cooling mechanisms when operating at high mainstream temperatures.

Additional analytical and experimental research is necessary to understand surface film stability under high turbulence and to predict the effectiveness of the vapor coolant downstream from the liquid.

Additional work in liquid film cooling is necessary in determining the most feasible velocity ratio of coolant to mainstream gas since film thickness and flow maldistribution aid instability.

LITERATURE CITED

1. Polytechnic Institute of Brooklyn, Brooklyn, New York, TRANSPIRATION COOLING OF A TURBULENT BOUNDARY LAYER IN AN AXISYMMETRICAL NOZZLE by Joseph Librizzi and Robert J. Cresci, February 1963, PIBAL Report No. 772, (AIAA Journal, Vol. 2, No. 4, April 1964, pp. 617-624) (Unclassified Report).

2. George P. Sutton, William R. Wagner, and J. D. Seader, ADVANCED COOLING TECHNIQUES FOR ROCKET ENGINES, Astronautics and Aeronautics, January 1966, pp. 60-71.

3. The Marquardt Corporation, Van Nuys, California, TRANSPIRATION-FILM COOLING STUDY USING SPIRAL-WOUND-RIBBON NOZZLES, February 1965, First Quarterly Progress Report, Report No. 25, 156, Contract No. AF 04(611)-10387 (Unclassified Report).

4. S. E. Colucci, COOLING METHODS FOR SOLID ROCKET NOZZLES, Chemical Engineering Techniques in Aerospace, Edited by D. J. Simkin, Chemical Engineering Progress, Vol. 60, Symposium Series, No. 52, 1964, pp. 116-129.

5. The Marquardt Corporation, Van Nuys, California, SPACECRAFT ENGINE THRUST CHAMBER COOLING - FINAL REPORT, 22 July 1964, Report No. 6069, N64-29196 (Unclassified Report).

6. Chemical Propellant Information Agency, John S. Hopkins University, Silver Springs, Maryland, LIQUID PROPELLANT ENGINE MANUAL (U), 5 November 1965, CPIA/M5 (Confidential Report).

7. F. Meyer - Hartwig, COOLING OF THERMALLY HIGH STRESSED SURFACES BY A COOLANT INTRODUCED THROUGH PORES IN THE MATERIAL (TRANSPIRATION CONSTRUCTION MATERIAL) (Kühlung hochhitzbeanspruchter Oberflüächen mit einem durch Poren im Werkstoff zugeführten Kühlmittel (Schwitzbaüstoffe)) Translated into English from the German by the Air Materiel Command, Report No. FB1470, 1 December 1940, Translation No. F-TS-2067-RE, ATI No. 22204 (Unclassified Report).

8. Massachusetts Institute of Technology, Naval Supersonic Laboratory, AN EXPERIMENT WITH A TRANSPIRATION-COOLED NOZZLE by Richard P. Bernicker, July 1960, AFOSR TN 60-1484, AD-254 260 (Unclassified Report).

9. Jet Propulsion Laboratory, PREPARATION AND PHYSICAL PROPERTIES OF POROUS METALS FOR SWEAT COOLING by P. Duwez and H. F. Martin, August 1947, Progress Report 3-14 (Unclassified Report).

10. Aerojet-General Corporation, Azusa, California, TRANSPIRATION COOLING AND FLOW-SEPARATION CONTROL BY GASEOUS INJECTION IN A POROUS NOZZLE (Supplement II to Final Report) by A. W. Magnusson, B. Misra, and W. R. Thompson, June 1961, AFFTC-TR-61-53, AD-263 458, AF 33(616)-5552 (Unclassified Report).

11. Aerojet-General Corporation, Sacramento, California, ADVANCED ROCKET ENGINE-STORABLE (U), Quarterly Technical Report for period July-September 1965, 15 October 1965, Report No. AFRPL-TR-65-189, AGC Report No. 10830-Q-1, Contract No. AF 04(611)-10830 (Confidential Report).

12. Air Force Materials Laboratory, Research and Technology Division, Air Force Systems Command, SELF-COOLED ROCKET NOZZLES by P. Schwarzkopf and E. D. Weisert, August 1965, Report No. RTD-TDR-63-4046, Vol. III, AD-473 691 (Unclassified Report).

13. United Nuclear Corporation, TRANSPIRATION AND FILM COOLING FOR SOLID PROPELLANT ROCKET NOZZLES by S. Hyman et al, 7 February 1961, Report No. NDA 2150-1, AD-273 333, Contract No. DA-30-069-0RD-3094 (Unclassified Report).

14. U. S. Naval Ordnance Test Station, China Lake, California, TRANSPIRATION COOLING WITH LIQUID METALS, PART 2: THEORETICAL DETERMINATION OF OPTIMUM COOLING PARAMETERS NEAR STAGNATION REGIONS by W. H. Thielbahr, August 1965, NAVWEPS Report No. 8732, NOTS TP3791 (Unclassified Report).

15. D. E. Rosner, TRANSPIRATION COOLING WITH CHEMICAL REACTIONS, Pyrodynamics, Vol. 2, May 1965, pp. 221-247.

16. Air Force Flight Dynamics Laboratory, Research and Technology Division, Air Force Systems Command, Wright-Patterson Air Force Base, Ohio, HYPERSONIC TURBULENT TRANSPIRATION COOLING INCLUDING DOWNSTREAM EFFECTS by L. W. Woodruff and G. C. Lorenz, June 1965, Technical Report No. AFFDL-TR-65-11 (Unclassified Report).

17. National Advisory Committee for Aeronautics, Washington, D. C., COMPARISON OF THE EFFECTIVENESS OF CONVECTION, TRANSPIRATION AND FILM COOLING METHODS WITH AIR AS COOLANT by E. R. G. Eckert and J. N. B. Livingood, 1954, Report No. NACA TR 1182 (Unclassified Report).

18. Massachusetts Institute of Technology, Cambridge, Massachusetts, HEAT, MASS, AND MOMENTUM TRANSFER FOR FLOW OVER A FLAT PLATE WITH BLOWING OR SUCTION by H. S. Mickley et al, September 1962 (Unclassified Report).

19. Rosemount Aeronautical Laboratories, University of Minnesota, MEASUREMENT OF RECOVERY FACTORS AND HEAT TRANSFER COEFFICIENTS WITH TRANSPIRATION COOLING IN A TURBULENT BOUNDARY LAYER AT M = 3 USING AIR AND HELIUM AS COOLANTS by B. M. Leadon and C. J. Scott, February 1956, Technical Report No. 126 (Unclassified Report).

20. National Advisory Committee for Aeronautics, Washington, D. C., THE EFFECT OF FLUID INJECTION ON THE COMPRESSIBLE TURBULENT BOUNDARY LAYER - PRELIMINARY TESTS ON TRANSPIRATION COOLING OF A FLAT PLATE AT M = 2.7 WITH AIR AS THE INJECTED GAS by Morris W. Rubesin, Constantine C. Pappas, and Arthur F. Okuno, 21 December 1955, NACA Research Memorandum A55I19 (Unclassified Report).

21. National Advisory Committee for Aeronautics, Washington, D. C., THE INFLUENCE OF SURFACE INJECTION ON HEAT TRANSFER AND SKIN FRICTION ASSOCIATED WITH THE HIGH-SPEED TURBULENT BOUNDARY LAYER by Morris W. Rubesin, 1955, NACA Research Memorandum A55L13 (Unclassified Report).

22. National Advisory Committee for Aeronautics, Washington, D. C., THE EFFECT OF FLUID INJECTION ON THE COMPRESSIBLE TURBULENT BOUNDARY LAYER - THE EFFECT OF SKIN FRICTION OF AIR INJECTED INTO THE BOUNDARY LAYER OF A CONE AT M = 2.7 by Thorval Tendeland and Arthur F. Okuno, June 1956, NACA Research Memorandum A56D05 (Unclassified Report).

23. National Advisory Committee for Aeronautics, MOMENTUM TRANSFER FOR FLOW OVER A FLAT PLATE WITH BLOWING by H. S. Mickley and R. S. Davis, November 1957, NACA Technical Note 4017 (Unclassified Report).

24. W. H. Dorrance and F. J. Dore, THE EFFECTS OF MASS TRANSFER ON COMPRESSIBLE TURBULENT BOUNDARY-LAYER SKIN-FRICTION AND HEAT TRANSFER, Journal of the Aerospace Sciences, Vol. 21, No. 6, June 1954, pp. 404-410.

25. J. P. Hartnett, D. J. Masson, J. F. Gross, and C. Gazley, Jr., MASS TRANSFER COOLING IN A TURBULENT BOUNDARY LAYER, IAS National Summer Meeting, Los Angeles, California, 28 June - 1 July 1960, ISA Paper No. 60-66.

26. National Advisory Committee for Aeronautics, AN ANALYTICAL ESTIMATION OF THE EFFECT OF TRANSPIRATION COOLING ON THE HEAT TRANSFER AND SKIN-FRICTION CHARACTERISTICS OF A COMPRESSIBLE, TURBULENT BOUNDARY LAYER by M. W. Rubesin, 1954, NACA Technical Note 3341 (Unclassified Report).

27. Rand Corporation, Santa Monica, California, ON MASS TRANSFER NEAR THE STAGNATION POINT by E. R. van Driest, Rand Symposium on Mass-Transfer Cooling for Hypersonic Flight, 1957 (Unclassified Proceedings).

28. Research and Technology Division, Wright-Patterson Air Force Base, Ohio, SUMMARY REPORT, SELF-COOLED ROCKET NOZZLES by F. B. Gessner, R. J. Ingram, and J. D. Scader, March 1964, Report No. RTD-TDR-63-4046, AD-601 574 (Unclassified Report).

29. F. B. Gessner, J. D. Seader, R. J. Ingram, and T. A. Coutlas, ANALYSIS OF SELF-COOLING WITH INFILTRATED POROUS TUNGSTEN COMPOSITES, Journal of Spacecraft and Rockets, Vol. 1, No. 6, November-December 1964, pp. 643-648.

30. Wright Air Development Division, Wright-Patterson Air Force Base, Ohio, TRANSIENT TEMPERATURE CHANGE IN SEMI-INFINITE POROUS SOLID WITH PHASE CHANGE AND TRANSPIRATION EFFECTS by R. J. Grosh, January 1960, TR 60-105 (Unclassified Report).

31. Purdue University, Jet Propulsion Center, Lafayette, Indiana, EFFECTS OF SELECTED GAS STREAM PARAMETERS AND COOLANT PHYSICAL PROPERTIES ON FILM COOLING OF ROCKET MOTORS by D. L. Emmons, August 1962, Report No. TM-62-5, Contract No. Nonr 1100(21) (AMSE Transactions-Journal of Heat Transfer, Vol 86, No. 2, May 1964, pp. 271-278) (Unclassified Report).

32. Air Force Institute of Technology, School of Engineering, Wright-Patterson Air Force Base, Ohio, AN EXPERIMENTAL INVESTIGATION OF NOZZLE COOLING FOR A SMALL ROCKET ENGINE by Donald J. Alser, August 1963, Master's Thesis (Unclassified Thesis).

33. Clifford D. Coulbert, SELECTING A THRUST CHAMBER COOLING TECHNIQUE FOR SPACECRAFT ROCKET ENGINES, American Institute of Aeronautics and Astronautics Summer Meeting, Los Angeles, California, 17-20 June 1963, AIAA Paper No. 63-241 (Unclassified Paper).

34. S. Ostrach and A. Koestel, FILM INSTABILITIES IN TWO-PHASE FLOWS, The Sixth National Heat Transfer Conference, Boston, Massachusetts, 11-14 April 1963 (Unclassified Proceeding).

35. Purdue University, Jet Propulsion Center, Lafayette, Indiana, ANALYTICAL AND EXPERIMENTAL INVESTIGATION OF FILM COOLING IN ROCKET NOZZLES by D. L. Crabtree, R. A. Gater, and C. F. Warner, 1964, N65-20353, Contract No. Nonr 1100(21) (ITS 1964 Review of Research, pp. 21-41).

36. S. S. Kutateladze and A. I. Leont'ev, FILM COOLING WITH A TURBULENT GASEOUS BOUNDARY LAYER, Thermal Physics High Temperature, January 1963, pp. 281-290.

37. J. P. Hartnett et al, VELOCITY DISTRIBUTIONS, TEMPERATURE DISTRIBUTIONS FOR AIR INJECTED THROUGH A TANGENTIAL SLOT INTO A TURBULENT BOUNDARY LAYER, ASME Transactions - Journal of Heat Transfer, Series C, Vol. 83, January 1961, pp. 293-306.

38. K. Wieghardt, HOT AIR DISCHARGE FOR DE-ICING (Foreign title not available) Translated into English from the German by the American Astronautical Federation, Translation F-TS-919-RE, December 1946 (Unclassified Report).

39. R. A. Seban, HEAT TRANSFER AND EFFECTIVENESS FOR A TURBULENT BOUNDARY LAYER WITH TANGENTIAL FLUID INJECTION, ASME Transactions - Journal of Heat Transfer, Series C, Vol. 83, 1961, pp. 293-306.

40. J. Chin et al, ADIABATIC WALL TEMPERATURE DOWNSTREAM OF A SINGLE INJECTION SLOT, ASME Paper No. 58-A-104, 1958 (Unclassified Paper).

41. J. Klein and M. Tribus, FORCED CONVECTION FROM NON-ISOTHERMAL SURFACES, University of Michigan Press, Ann Arbor, Michigan, 1953 (Heat Transfer Symposium).

42. Lewis Research Center, NASA, Cleveland, Ohio, USE OF A THEORETICAL FLOW MODEL TO CORRELATE DATA FOR FILM COOLING OR HEATING AN ADIABATIC WALL BY TANGENTIAL INJECTION OF GASES AT DIFFERENT FLUID PROPERTIES by James E. Hatch and S. Stephen Papell, 1959, Report No. NASA TN D-130 (Unclassified Report).

43. D. B. Spalding, PREDICTION OF ADIABATIC WALL TEMPERATURES IN FILM-COOLING SYSTEMS, AIAA Journal, Vol. 3, No. 5, May 1965, pp. 965-967.

44. J. L. Stollery and A. A. M. El-Ehwany, A NOTE ON THE USE OF A BOUNDARY-LAYER MODEL FOR CORRELATING FILM-COOLING DATA, International Journal of Heat Mass Transfer, Vol. 8, January 1965, pp. 55-56.

45. R. A. Seban and I. H. Back, VELOCITY AND TEMPERATURE PROFILES IN TURBULENT BOUNDARY LAYERS WITH TANGENTIAL INJECTION, ASME Transactions - Journal of Heat Transfer, Series C, Vol. 84, 1962, pp. 45-54.

46. Aeronautics Department, Imperial College, England, Unpublished Work of J. Stollery, 1962.

47. Lewis Research Center, NASA, Cleveland, Ohio, AN EXPERIMENTAL INVESTIGATION OF GASEOUS-FILM COOLING OF A ROCKET MOTOR by James G. Lucas and Richard L. Golladay, October 1963, NASA TN D-1988, N63-21895 (Unclassified Report).

48. Naval Ordnance Laboratory, White Oak, Maryland, AIR-FILM COOLING OF A SUPERSONIC NOZZLE by Bing H. Lien, August 1964, Aerodynamic Research Report No. 224, NOLTR 64-65, N64-31672, AD-448 477 (Unclassified Report).

49. S. E. Colucci, L. Kurylko, and C. George, SOLID ROCKET COOLING (U), Proceedings of the Fifth U. S. Navy Symposium on Aeroballistics, Vol. II, October 1961, (Confidential Proceedings).

50. Lewis Research Center, NASA, Cleveland, Ohio, EFFECT OF GASEOUS FILM COOLING OF COOLANT INJECTION THROUGH ANGLED SLOTS AND NORMAL HOLES by S. Stephen Papell, September 1960, NASA TN D-299 (Unclassified Report).

51. John P. Sellers, Jr., GASEOUS FILM COOLING WITH MULTIPLE INJECTION STATIONS, AIAA Journal, Vol. 1, No. 9, September 1963, pp. 2154-2156.

52. Allison Division, General Motors Corporation, Indianapolis, Indiana, DEVELOPMENT OF COOLING SYSTEM FOR SOLID ROCKET NOZZLES - FINAL TECHNICAL REPORT (U), 15 November 1962, Engineering Department, Report No. 2994, Contract No. AF 04(611)-5691 (Confidential Report).

53. Aerojet-General Corporation, Sacramento, California, HIGH CHAMBER PRESSURE ROCKETRY PROGRAM (U), 22 February 1965, Quarterly Progress Report 8191-Q-11, Contract No. AF 04(611)-8191 (Confidential Report).

54. The Marquardt Corporation, Van Nuys, California, THRUST CHAMBER COOLING TECHNIQUES FOR SPACECRAFT ENGINES-FINAL REPORT, 15 July 1963, NASA CR-50959, N63-21074, Contract No. NAS-7-103, (Unclassified Report).

55. The Marquardt Corporation, Van Nuys, California, RAMJET STRUCTURAL ELEMENTS AND NONREGENERATIVELY COOLED COMBUSTION CHAMBERS AND NOZZLES (U), August 1964, Report No. X64-17794, AD-351421, Contract No. AF 33(657)-12146, (Vol. 9 of "Final Summary Technical Report on the Calendar Year 1963 Ramjet Technology Program" (U) (Confidential Report).

DISTRIBUTION

EXTERNAL

	No. of Copies
Air University Library ATTN: AUL3T Maxwell Air Force Base, Alabama 36112	1
U. S. Army Electronics Proving Ground ATTN: Technical Library Fort Huachuca, Arizona	1
U. S. Naval Ordnance Test Station ATTN: Technical Library, Code 753 China Lake, California 93555	1
U. S. Naval Ordnance Laboratory ATTN: Library Corona, California 91720	1
Lawrence Radiation Laboratory ATTN: Technical Information Division P. O. Box 808 Livermore, California	1
Sandia Corporation ATTN: Technical Library P. O. Box 969 Livermore, California 94551	1
U. S. Naval Postgraduate School ATTN: Library Monterey, California 93940	1
Electronic Warfare Laboratory, USAECOM Post Office Box 205 Mountain View, California 94042	1
Jet Propulsion Laboratory ATTN: Library (TDS) 4800 Oak Grove Drive Pasadena, California 91103	2
U. S. Naval Missile Center ATTN: Technical Library, Code N3022 Point Mugu, California	1
U. S. Army Air Defense Command ATTN: ADSX Ent Air Force Base, Colorado 80912	1
Central Intelligence Agency ATTN: OCR/DD-Standard Distribution Washington, D. C. 20505	4
Harry Diamond Laboratories ATTN: Library Washington, D. C. 20438	1
Scientific & Tech. Information Div., NASA ATTN: ATS Washington, D. C. 20546	1
U. S. Atomic Energy Commission ATTN: Reports Library, Room G-017 Washington, D. C. 20545	1
U. S. Naval Research Laboratory ATTN: Code 2027 Washington, D. C. 20390	1
Weapons Systems Evaluation Group Washington, D. C. 20305	1
John F. Kennedy Space Center, NASA ATTN: KSC Library, Documents Section Kennedy Space Center, Florida 32899	2
APGC (PGBPS-12) Eglin Air Force Base, Florida 32542	1
U. S. Army CDC Infantry Agency Fort Benning, Georgia 31905	1
Argonne National Laboratory ATTN: Report Section 9700 South Cass Avenue Argonne, Illinois 60440	1
U. S. Army Weapons Command ATTN: AMSWE-RDR Rock Island, Illinois 61201	1
Rock Island Arsenal ATTN: SWERI-RDI Rock Island, Illinois 61201	1
U. S. Army Cmd. & General Staff College ATTN: Acquisitions, Library Division Fort Leavenworth, Kansas 66027	1
Combined Arms Group, USACDC ATTN: Op. Res., P and P Div. Fort Leavenworth, Kansas 66027	1
U. S. Army CDC Armor Agency Fort Knox, Kentucky 40121	1
Michoud Assembly Facility, NASA ATTN: Library, I-MICH-OSD P. O. Box 29300 New Orleans, Louisiana 70129	1
Aberdeen Proving Ground ATTN: Technical Library, Bldg. 313 Aberdeen Proving Ground, Maryland 21005	1
NASA Sci. & Tech. Information Facility ATTN: Acquisitions Branch (S-AK/DL) P. O. Box 33 College Park, Maryland 20740	5
U. S. Army Edgewood Arsenal ATTN: Librarian, Tech. Info. Div. Edgewood Arsenal, Maryland 21010	1

	No. of Copies
National Security Agency ATTN: C3/TDL Fort Meade, Maryland 20755	1
Goddard Space Flight Center, NASA ATTN: Library, Documents Section Greenbelt, Maryland 20771	1
U. S. Naval Propellant Plant ATTN: Technical Library Indian Head, Maryland 20640	1
U. S. Naval Ordnance Laboratory ATTN: Librarian, Eva Liberman Silver Spring, Maryland 20910	1
Air Force Cambridge Research Labs. L. G. Hanscom Field ATTN: CRMXLR/Stop 29 Bedford, Massachusetts 01730	1
Springfield Armory ATTN: SWESP-RE Springfield, Massachusetts 01101	1
U. S. Army Materials Research Agency ATTN: AMXMR-ATL Watertown, Massachusetts 02172	1
Strategic Air Command (OAI) Offutt Air Force Base, Nebraska 68113	1
Picatinny Arsenal, USAMUCOM ATTN: SMUPA-VA6 Dover, New Jersey 07801	1
U. S. Army Electronics Command ATTN: AMSEL-CB Fort Monmouth, New Jersey 07703	1
Sandia Corporation ATTN: Technical Library P. O. Box 5800 Albuquerque, New Mexico 87115	1
ORA(RRRT) Holloman Air Force Base, New Mexico 88330	1
Los Alamos Scientific Laboratory ATTN: Report Library P. O. Box 1663 Los Alamos, New Mexico 87544	1
White Sands Missile Range ATTN: Technical Library White Sands, New Mexico 88002	1
Rome Air Development Center (EMLAL-1) ATTN: Documents Library Griffiss Air Force Base, New York 13440	1
Brookhaven National Laboratory Technical Information Division ATTN: Classified Documents Group Upton, Long Island, New York	1
Watervliet Arsenal ATTN: SWEWV-RD Watervliet, New York 12189	1
U. S. Army Research Office (ARO-D) ATTN: CRD-AA-IP Box CM, Duke Station Durham, North Carolina	1
Lewis Research Center, NASA ATTN: Library 21000 Brookpark Road Cleveland, Ohio 44135	1
Systems Engineering Group (RTD) ATTN: SEPIR Wright-Patterson Air Force Base, Ohio 45433	1
U. S. Army Artillery & Missile School ATTN: Guided Missile Department Fort Sill, Oklahoma 73503	1
U. S. Army CDC Artillery Agency ATTN: Library Fort Sill, Oklahoma 73504	1
U. S. Army War College ATTN: Library Carlisle Barracks, Pennsylvania 17013	1
U. S. Naval Air Development Center ATTN: Technical Library Johnsville, Warminster, Pennsylvania 18974	1
Frankford Arsenal ATTN: C-2500-Library Philadelphia, Pennsylvania 19137	1
Div. of Technical Information Ext., USAEC P. O. Box 62 Oak Ridge, Tennessee	1
Oak Ridge National Laboratory ATTN: Central Files P. O. Box X Oak Ridge, Tennessee	1
Air Defense Agency, USACDC ATTN: Library Fort Bliss, Texas 79916	1
U. S. Army Air Defense School ATTN: AKBAAS-DR-R Fort Bliss, Texas 79906	1

	No. of Copies
U. S. Army CDC Nuclear Group Fort Bliss, Texas 79916	1
Manned Spacecraft Center, NASA ATTN: Technical Library, Code BM6 Houston, Texas 77058	1
Defense Documentation Center Cameron Station Alexandria, Virginia 22314	20
U. S. Army Research Office ATTN: STINFO Division 3045 Columbia Pike Arlington, Virginia 22204	1
U. S. Naval Weapons Laboratory ATTN: Technical Library Dahlgren, Virginia 22448	1
U. S. Army Engineer Res. & Dev. Labs. ATTN: Scientific & Technical Info. Br. Fort Belvoir, Virginia 22060	2
Langley Research Center, NASA ATTN: Library, MS-185 Hampton, Virginia 23365	1
Research Analysis Corporation ATTN: Library McLean, Virginia 22101	1

INTERNAL

	No. of Copies
Headquarters U. S. Army Missile Command Redstone Arsenal, Alabama	
ATTN: AMSMI-D	1
AMSMI-XE, Mr. Lowers	1
AMSMI-XS, Dr. Carter	1
AMSMI-Y	1
AMSMI-R, Mr. McDaniel	1
AMSMI-RAP	1
AMSMI-RBLD	10
USACDC-LnO	1
AMSMI-RBR	25
AMSMI-RB, Mr. Croxton	1
AMSMI-RKL, Mr. Connaughton	12
AMSMI-RT	1
AMSMI-RF	1
AMSMI-RS	1
AMSMI-R, Mr. Fagan	1
AMSMI-RR, Dr. Hallows	1
AMCPM-NX, Dr. Lange	1

	No. of Copies
National Aeronautics & Space Administration Marshall Space Flight Center Redstone Arsenal, Alabama	
ATTN: MS-T, Mr. Wiggins	5
I-E-MGR	1
R-P&VE-P	1
R-P&VE-PTE, Mr. Patterson	1
DIR, Mr. Shepherd	1
R-RP-N, Dr. Shelton	1
MS-CH, Mr. Sorensen	1
I-PL-CH, Mr. Goodrum	1